

# Online Research @ Cardiff

This is an Open Access document downloaded from ORCA, Cardiff University's institutional repository: <https://orca.cardiff.ac.uk/id/eprint/109926/>

This is the author's version of a work that was submitted to / accepted for publication.

Citation for final published version:

Van Braeckel-Budimir, Natalija, Gras, Stephanie, Ladell, Kristin ORCID: <https://orcid.org/0000-0002-9856-2938>, Josephs, Tracy M., Pewe, Lecia, Urban, Stina L., Miners, Kelly L., Farenc, Carine, Price, David A. ORCID: <https://orcid.org/0000-0001-9416-2737>, Rossjohn, Jamie ORCID: <https://orcid.org/0000-0002-2020-7522> and Harty, John T. 2017. A T cell receptor locus harbors a malaria-specific immune response gene. Immunity 47 (5) , 835-847.e4. 10.1016/j.immuni.2017.10.013 file

Publishers page: <http://dx.doi.org/10.1016/j.immuni.2017.10.013>  
<<http://dx.doi.org/10.1016/j.immuni.2017.10.013>>

Please note:

Changes made as a result of publishing processes such as copy-editing, formatting and page numbers may not be reflected in this version. For the definitive version of this publication, please refer to the published source. You are advised to consult the publisher's version if you wish to cite this paper.

This version is being made available in accordance with publisher policies.

See

<http://orca.cf.ac.uk/policies.html> for usage policies. Copyright and moral rights for publications made available in ORCA are retained by the copyright holders.



# **A T cell receptor locus encodes a malaria-specific immune response gene**

**Natalija Van Braeckel-Budimir<sup>1\*</sup>, Stephanie Gras<sup>2,3\*</sup>, Kristin Ladell<sup>4\*</sup>,  
Tracy M. Josephs<sup>2,3</sup>, Lecia Pewe<sup>1</sup>, Stina L. Urban<sup>1</sup>, Kelly L. Miners<sup>4</sup>,  
Carine Farenc<sup>3</sup>, David A. Price<sup>4,5+</sup>, Jamie Rossjohn<sup>2,3,4+</sup>, John T. Harty<sup>1,6,7+</sup>**

Running title: An *Ir* gene in a TCR locus

<sup>1</sup>Department of Microbiology, University of Iowa, Iowa City, IA 52242, USA;

<sup>2</sup>Australian Research Council Centre of Excellence for Advanced Molecular Imaging, Monash University, Clayton, Victoria 3800, Australia;

<sup>3</sup>Infection and Immunity Program and Department of Biochemistry and Molecular Biology, Biomedicine Discovery Institute, Monash University, Clayton, Victoria 3800, Australia;

<sup>4</sup>Division of Infection and Immunity, Cardiff University School of Medicine, Cardiff CF14 4XN, UK;

<sup>5</sup>Human Immunology Section, Vaccine Research Center, National Institute of Allergy and Infectious Diseases, National Institutes of Health, Bethesda, MD 20892, USA;

<sup>6</sup>Department of Pathology, University of Iowa, Iowa City, IA 52242, USA;

<sup>7</sup>Interdisciplinary Program in Immunology, University of Iowa, Iowa City, IA 52242, USA.

\*These authors contributed equally.

<sup>+</sup>Senior authors.

Correspondence: JTH ([john-harty@uiowa.edu](mailto:john-harty@uiowa.edu)), JR ([jamie.rossjohn@monash.edu](mailto:jamie.rossjohn@monash.edu)) or DAP ([priced6@cardiff.ac.uk](mailto:priced6@cardiff.ac.uk)).

Lead contact: JTH ([john-harty@uiowa.edu](mailto:john-harty@uiowa.edu)).

## SUMMARY

Immune response (*Ir*) genes, originally proposed by Baruj Benacerraf to explain differential antigen-specific responses in animal models, have become synonymous with the major histocompatibility complex (MHC). We discovered a non-MHC-linked *Ir* gene in a T cell receptor (TCR) locus that was required for CD8<sup>+</sup> T cell responses to the *Plasmodium berghei* GAP50<sub>40-48</sub> epitope in mice expressing the MHC class I allele H-2D<sup>b</sup>. GAP50<sub>40-48</sub>-specific CD8<sup>+</sup> T cell responses emerged from a very large pool of naive Vβ8.1<sup>+</sup> precursors, which dictated susceptibility to cerebral malaria and conferred protection against recombinant *Listeria monocytogenes* infection. Structural analysis of a prototypical Vβ8.1<sup>+</sup> TCR-H-2D<sup>b</sup>-GAP50<sub>40-48</sub> ternary complex revealed that germline-encoded complementarity-determining region 1β residues present exclusively in the Vβ8.1 segment mediated essential interactions with the GAP50<sub>40-48</sub> peptide. Collectively, these findings demonstrated that *Vβ8.1* functioned as an *Ir* gene that was indispensable for immune reactivity against the malaria GAP50<sub>40-48</sub> epitope.

## KEY WORDS

Immune response genes; TCR bias; naive CD8<sup>+</sup> T cells; malaria; experimental cerebral malaria.

## INTRODUCTION

Genetic regulation of the immune system is a central determinant of health and disease. Based on the observation that random-bred guinea pigs challenged with simple antigens segregate into responder and non-responder groups, Benacerraf and colleagues proposed the notion of autosomal dominant immune response (*Ir*) genes (Benacerraf and Germain, 1978). *Ir* genes were first identified as major histocompatibility complex (MHC)-linked (McDevitt and Chinitz, 1969), and subsequently found to encode specific allotypes of antigen-presenting molecules, such as MHC class II (MHC II) (Benacerraf, 1974; Benacerraf and McDevitt, 1972). Although unidentified at the time, a determinative role was also suggested for the putative T cell receptor (TCR) (Benacerraf and Germain, 1978). MHC II-mediated antigen presentation is required to activate T helper cells and generate antibody responses to T-dependent antigens (Owens and Zeine, 1989). In addition, the host must assemble TCRs capable of engaging specific MHC-peptide (MHCp) complexes with sufficient avidity to trigger immune reactivity (Davis et al., 2003; van der Merwe and Dushek, 2011). Numerous studies of inbred animals have linked the absence of specific immune responses with a lack of appropriate MHC alleles (Marshak et al., 1977; Zinkernagel, 1978). In contrast, despite major advances in our understanding of antigen recognition over the last four decades, it remains unclear if germline-encoded segments of the TCR can function as *Ir* genes.

CD8<sup>+</sup> T cells recognize MHC I-restricted peptides via heterodimeric TCRs (Davis and Bjorkman, 1988; Townsend et al., 1985). A vast number of different TCRs can be generated from a limited number of germline-encoded segments through the process of *V(D)J* gene recombination with junctional diversification and subsequent random pairing of the somatically rearranged TCR $\alpha$  and TCR $\beta$  chains (Cabaniols et al., 2001; Chothia et al., 1988; Davis and Bjorkman, 1988; Rossjohn et al., 2015; Turner et al., 2006). As a consequence, each individual harbors an extensive repertoire of naive CD8<sup>+</sup> T cells, which ensures broad recognition of a large number of foreign antigens presented by MHC I (Goldrath and Bevan, 1999). To meet the diversity criterion within space limitations, however, only a few naive precursors are specific for any given epitope (Blattman et al., 2002; Obar et al., 2008), and robust antigen-driven proliferation is

required to establish effector and memory CD8<sup>+</sup> T cell populations (Busch et al., 1998; Goldrath and Bevan, 1999). It is estimated that most naive antigen-specific repertoires in mice do not contain more than 10–300 CD8<sup>+</sup> T cells (Obar et al., 2008). Larger pre-immune repertoires comprising 1,000–1,500 naive CD8<sup>+</sup> T cells have been reported for the murine cytomegalovirus (MCMV) M45<sub>985-993</sub> and vaccinia virus (VacV) B8R<sub>20-27</sub> epitopes (Jenkins and Moon, 2012), but it remains unclear if these specific precursor pools define the upper limits of antigen reactivity in the post-thymic landscape of clonotypically distributed TCRs.

Clonal selection ensures the recruitment of biologically and structurally optimal immune receptors from the naive repertoire (Malherbe et al., 2004; Price et al., 2005), frequently leading to biased TCR usage among memory CD8<sup>+</sup> T cell populations (Miles et al., 2011; Turner et al., 2006). In extreme cases, non-peptidic antigens restricted by non-classical MHC molecules elicit innate-like responses dominated by semi-invariant TCRs (Bendelac et al., 1997; Godfrey et al., 2015; Van Rhijn et al., 2015). Here, we found that a similar phenomenon can regulate conventional CD8<sup>+</sup> T cell immunity. We demonstrated that an epitope from the *Plasmodium berghei* (*P. berghei*) ANKA glideosome-associated protein (GAP50<sub>40-48</sub>), a key pathogenic target in experimental cerebral malaria (ECM), was associated with the largest naive CD8<sup>+</sup> T cell repertoire yet described in laboratory mice (Jenkins and Moon, 2012). We also revealed the molecular properties of these GAP50<sub>40-48</sub>-specific TCRs, demonstrating exclusive use of the V $\beta$ 8.1 segment underpinned by direct interactions with the malarial peptide. Mice lacking the V $\beta$ 8.1 gene did not respond to the GAP50<sub>40-48</sub> epitope after *P. berghei* infection and did not develop ECM. Moreover, the very large pool of naive precursors conferred enhanced control of primary infection with recombinant *Listeria monocytogenes* (*L. monocytogenes*) expressing the GAP50<sub>40-48</sub> epitope. Collectively, these findings extend the notion of *Ir* genes to incorporate germline-encoded components of antigen-specific TCRs.

## RESULTS

### **GAP50<sub>40-48</sub>-specific CD8<sup>+</sup> T cells exhibit an extreme TCR bias**

ECM in susceptible C57Bl/6 (B6) mice infected with *P. berghei* ANKA (Engwerda et al., 2005) is a valuable model of severe malarial disease (Brewster et al., 1990). It is established that the development of ECM is critically dependent on pathogenic CD8<sup>+</sup> T cells (Amani et al., 2000; Haque et al., 2011; Yanez et al., 1996) expressing V $\beta$ 8<sup>+</sup> TCRs (Boubou et al., 1999; Mariotti-Ferrandiz et al., 2016), especially those specific for the H-2D<sup>b</sup>-restricted GAP50<sub>40-48</sub> epitope (Howland et al., 2013). However, it is not known why GAP50<sub>40-48</sub>-specific CD8<sup>+</sup> T cells are pathogenic in ECM. To address this issue, we set out to generate TCR retrogenic mice harboring monoclonal or oligoclonal CD8<sup>+</sup> T cell populations specific for individual epitopes derived from *P. berghei*, namely thrombospondin-related adhesion protein (TRAP)<sub>130-138</sub>, sporozoite-specific protein 20 (S20)<sub>318-326</sub> and GAP50<sub>40-48</sub> (Holst et al., 2006; Hafalla et al., 2013; Howland et al., 2013). As a first step, we immunized three separate groups of B6 mice with peptide-pulsed dendritic cells (DCs) followed 7 days later by recombinant *L. monocytogenes* expressing the same epitope (LM-GAP50<sub>40-48</sub>). This accelerated prime-boost approach (Badovinac et al., 2005) elicited large CD8<sup>+</sup> T cell responses specific for TRAP<sub>130-138</sub>, S20<sub>318-326</sub> and GAP50<sub>40-48</sub> (Fig. S1A). We then used the corresponding MHC I tetramers and a panel of anti-mouse V $\beta$  antibodies to profile the constituent malaria-specific TCRs.

CD8<sup>+</sup> T cells specific for TRAP<sub>130-138</sub> and S20<sub>318-326</sub> expressed several different TCR V $\beta$  segments with distinct preferences (Fig. 1A and S1B). For example, almost 75% of the S20<sub>318-326</sub>-specific repertoire was focused on V $\beta$ 8.1/8.2 and V $\beta$ 8.3, while the TRAP<sub>130-138</sub>-specific repertoire was dominated by V $\beta$ 2 and V $\beta$ 7. In contrast, >99% of GAP50<sub>40-48</sub>-specific CD8<sup>+</sup> T cells expressed V $\beta$ 8.1/8.2, which cannot be discriminated by antibody staining (Fig. 1A and S1B). These segments comprised <15% of the corresponding GAP50<sub>40-48</sub> tetramer<sup>-</sup> repertoires in the same mice (Fig. 1B). Moreover, an identical TCR bias was observed after inoculation of sporozoites by mosquito bite or immunization with radiation-attenuated sporozoites or DC-GAP50<sub>40-48</sub> alone (data not shown), and similar results were obtained with other strains of mice expressing the

MHC I allele H-2D<sup>b</sup>, including CB6F1 and BALB.b (Fig. S1C). The GAP50<sub>40-48</sub> epitope therefore mobilized an almost exclusive repertoire of TCR V $\beta$ -defined memory CD8<sup>+</sup> T cells.

To gain a deeper understanding of this extreme bias, we sorted GAP50<sub>40-48</sub>-specific CD8<sup>+</sup> T cells directly *ex vivo* from DC-LM-GAP50<sub>40-48</sub>-immunized B6 mice and performed an unbiased molecular analysis of all expressed *TRA* and *TRB* gene rearrangements (Quigley et al., 2011). Sequence analysis showed that >98% of transcripts encoded V $\beta$ 8.1 (Fig. 1C and Table S1). In contrast, a variety of *TRAV* gene segments were detected, indicating promiscuous pairing of diverse TCR $\alpha$  chains with a constrained repertoire of V $\beta$ 8.1<sup>+</sup> TCR $\beta$  chains (Fig. 1D). Almost 40% of retrogenic T cells generated with a GAP50<sub>40-48</sub>-specific TCR $\beta$  chain bound the GAP50<sub>40-48</sub> tetramer in naive mice, while only ~1% of retrogenic T cells generated with a TRAP<sub>130-138</sub>-specific TCR $\beta$  chain bound the TRAP<sub>130-138</sub> tetramer (Fig. S2). These data suggested that the V $\beta$ 8.1 segment was a major recognition element for GAP50<sub>40-48</sub>-specific CD8<sup>+</sup> T cells.

Analysis of the third TCR $\beta$  chain complementarity-determining region (CDR3 $\beta$ ) revealed additional features of the GAP50<sub>40-48</sub>-specific repertoire (Fig. S3A–C, Table S1). In particular, we identified a common CDR3 $\beta$  length (~60% of translated sequences incorporated 14 amino acids) (Fig. S3A), an almost uniform bias towards *TRBD2* gene usage within a single reading frame (Fig. S3B) and a strong preference for *TRBJ* gene segments from the J $\beta$ 2 cluster (Fig. S3C). Moreover, the V $\beta$ -D $\beta$  junction lacked N additions, and a germline-encoded CDR3 $\beta$  motif (<sup>104</sup>CASSDWG<sup>110</sup>) was present in >95% of sequences (Table S1 and Fig. 1E). These data demonstrated that a highly convergent pattern of gene rearrangements “licensed” the V $\beta$ 8.1-driven immune response to the GAP50<sub>40-48</sub> epitope (Quigley et al., 2010).

### **The C-terminal region of the GAP50<sub>40-48</sub> peptide is a “hotspot” for TCR recognition**

To understand the molecular basis of this extreme TCR bias, we first determined the structure of the H-2D<sup>b</sup>-GAP50<sub>40-48</sub> complex at a resolution of 2.2 Å (Table S2). The bound peptide adopted a canonical extended conformation (Young et al., 1994), with four solvent-exposed amino acid residues (P4-L, where L is leucine; P6-A, where A is

alanine; P7-K, where K is lysine; and P8-Y, where Y is tyrosine) representing potential contacts for the TCR (Fig. 2A).

To determine which GAP50<sub>40-48</sub> residues were important for TCR recognition, we replaced individual amino acids with alanine (Ala), except for the wildtype (*wt*) Ala residue at position 6 (P6), which was replaced with serine (Ser) (Fig. 2B). We did not mutate the critical H-2D<sup>b</sup> anchor residues at P5 or P9 (Valkenburg et al., 2013). The *wt* and mutant peptides were then used at saturating concentrations in intracellular cytokine staining assays to determine the impact of each residue on the functional reactivity of GAP50<sub>40-48</sub>-specific CD8<sup>+</sup> T cells (Fig. 2C and S4). Interferon- $\gamma$  (IFN $\gamma$ ) production relative to the *wt* peptide was unaffected by the substitutions at P1, P2 and P3 (Fig. 2C). In contrast, the mutations at P4-L and P6-A diminished IFN $\gamma$  production, while the mutations at P7-K and P8-Y abolished IFN $\gamma$  production (Fig. 2C). The C-terminal P7-K and P8-Y residues were therefore crucial for GAP50<sub>40-48</sub>-specific CD8<sup>+</sup> T cell activation and represented “hotspots” for TCR engagement (Fig. 2D).

### **GAP50<sub>40-48</sub> peptide “hotspots” interact exclusively with the TCR $\beta$ chain**

Next, we determined the structure of a prototypical V $\beta$ 8.1<sup>+</sup> TCR, derived from the GAP50<sub>40-48</sub>-specific CD8<sup>+</sup> T cell clone NB1 (Table S3), in complex with H-2D<sup>b</sup>-GAP50<sub>40-48</sub> (Fig. 3A, Table S2). The NB1 TCR docked centrally atop the H-2D<sup>b</sup> cleft, with an angle of 43° and a buried surface area (BSA) of approximately 2,200 Å<sup>2</sup>, values that fall within the range previously determined for TCR-MHCp complexes (Rossjohn et al., 2015) (Fig. 3B). All six CDR loops were involved to a varying extent in the interaction with H-2D<sup>b</sup>-GAP50<sub>40-48</sub> (Fig. 3C). Namely, the CDR3 $\alpha$  and CDR3 $\beta$  loops contributed 24% and 20% of the BSA, respectively, while the CDR1 $\alpha$  and CDR2 $\alpha$  loops each contributed ~17% of the BSA (Fig. 3C). Somewhat unexpectedly given the extreme TCR V $\beta$  bias, the germline-encoded CDR1 $\beta$  and CDR2 $\beta$  loops each contributed only ~10% of the BSA. Thus, the cumulative  $\beta$  chain contribution to the overall BSA was substantially smaller (39%) relative to the cumulative  $\alpha$  chain contribution (61%) (Fig. 3C). However, >95% of TCR-GAP50<sub>40-48</sub> peptide interactions were mediated by the TCR $\beta$  chain (Fig. 3D, Table S4), while the TCR $\alpha$  chain primarily contacted the MHC molecule (74% of the BSA) (Fig. 3E, Table S4).



The CDR1 $\alpha$  loop stretched between the peptide-binding  $\alpha$ -helices of H-2D<sup>b</sup>, with tyrosine (Tyr) 28 $\alpha$  playing a principal role by contacting glutamic acid (Glu)163, Glu166 and tryptophan (Trp)167 at the N-terminal end of the cleft (Fig. 3F, Table S4). The CDR2 $\alpha$  loop sat above the  $\alpha$ 2-helix, with arginine (Arg)57 $\alpha$  lying flat above residues Glu154 and Ala158 (Fig. 3G). The CDR3 $\alpha$  loop contacted a large stretch of the  $\alpha$ 1-helix (spanning residues 58–72), with hydrophobic and hydrogen bond contacts exclusively mediated by germline-encoded residues from the J $\alpha$  segment (<sup>108</sup>Y<sup>109</sup>AQ<sup>110</sup>, where Q is glutamine) (Fig. 3H). The NB1 TCR $\alpha$  chain engaged the H-2D<sup>b</sup> molecule with a large footprint over the N-terminal region of the antigen-binding cleft (Fig. 3B). Mutational analyses of H-2D<sup>b</sup> binding performed using three distinct GAP50<sub>40-48</sub>-specific CD8<sup>+</sup> T cell clones further indicated that different V $\beta$ 8.1<sup>+</sup> TCRs used an identical MHC I docking strategy (Fig. S5, Table S5).

Interactions between the NB1 TCR $\alpha$  chain and the GAP50<sub>40-48</sub> peptide were limited to two van der Waals interactions between the CDR3 $\alpha$  loop and P4-L (Table S4). In contrast, the NB1 TCR V $\beta$ 8.1 region dominated contacts with the bound epitope (44 of 46 contacts) (Table S4). Moreover, all three CDR $\beta$  loops contacted the C-terminus of the peptide (P6–8) (Fig. 3I–K), encompassing the previously identified “hotspots” for CD8<sup>+</sup> T cell recognition (Fig. 2D). The CDR1 $\beta$  loop interacted with both P7-K and P8-Y via its <sup>28</sup>N-DY<sup>31</sup> motif (where N is asparagine and D is aspartic acid). More specifically, P7-K and P8-Y formed a notch in which aspartic acid (Asp)30 $\beta$  was inserted as a peg, forming a salt bridge with P7-K (Fig. 3J). In addition, asparagine (Asn)28 $\beta$  hydrogen bonded via its main chain with P7-K, while the aromatic group of Tyr31 $\beta$  sat above P8-Y (Fig. 3J). Contacts were also established between P8-Y and the CDR2 $\beta$  loop via Tyr57. Accordingly, P8-Y was closely sequestered upon TCR binding (Fig. 3J). The conserved CDR3 $\beta$  motif <sup>108</sup>DW<sup>109</sup> (where W is tryptophan), which was most frequently germline-encoded within the *D* gene (Fig. 1E), interacted with P6-A and P7-K (Fig. 3K). The large Trp109 $\beta$  side chain lay flat on the top of P6-A, acting as a lid covering the central part of the epitope, while Asp108 $\beta$  and P7-K formed a salt bridge (Fig. 3K).

TCR $\beta$  chain interactions with the H-2D<sup>b</sup> molecule were modest in comparison to the TCR $\alpha$  chain (Table S4). The CDR1 $\beta$  loop contacted only glutamine (Gln)72 via Tyr31 $\beta$  (Fig. 3I, J). The side chains of valine (Val)58 $\beta$  from the CDR2 $\beta$  loop abutted

Val76 from H-2D<sup>b</sup>, establishing an interaction network extended by Tyr57 $\beta$ -mediated contacts with Gln72, Arg75 and Val76. The conserved CDR3 $\beta$ <sup>108</sup>DW<sup>109</sup> motif from the *TRBD2* gene segment formed interactions with the hinge region of the  $\alpha$ 2-helix, whereby Trp109 $\beta$  nestled between histidine (His)155 and Ser150. Thus, germline-encoded TCR $\beta$  chain residues played a minor role in contacting the H-2D<sup>b</sup> molecule.

The observation that the prototypical NB1 TCR interacted with GAP50<sub>40-48</sub> extensively via its  $\beta$  chain suggested that the peptide itself drove the extreme bias towards V $\beta$ 8.1. This notion contrasts with prevailing dogma, which asserts that germline bias arises as a consequence of allotype-specific MHC reactivity (Garcia et al., 2009).

### **CDR1 residues unique to V $\beta$ 8.1 are critical for GAP50<sub>40-48</sub> peptide recognition**

These structural insights allowed us to identify candidate factors underlying the exclusive recruitment of V $\beta$ 8.1<sup>+</sup> TCR clonotypes into the immune repertoire. To determine the precise amino acid sequences involved in this process, we initially focused on the germline-encoded CDR1 $\beta$  and CDR2 $\beta$  loops. Sequence alignments revealed that the CDR1 $\beta$  loops encoded by six *TRBV* genes shared a common Asp30 $\beta$ , while the Asp30 $\beta$ -Tyr31 $\beta$  motif was unique to V $\beta$ 8.1. In the other five *TRBV* genes, Tyr31 $\beta$  was replaced by a smaller threonine (Thr)/Ser residue (Table S6A). Three *TRBV* genes shared a common Val58 $\beta$  residue in the encoded CDR2 $\beta$  loop, but only V $\beta$ 8.1 incorporated the additional Tyr57 $\beta$  required to sequester P8-Y (Table S6B).

Although the conserved CDR3 $\beta$  region interacted with both the peptide and H-2D<sup>b</sup>, we wanted to determine if the germline-encoded V $\beta$ 8.1 residues were essential for TCR-mediated recognition of H-2D<sup>b</sup>-GAP50<sub>40-48</sub>. We therefore conducted affinity measurement studies using targeted mutants of the NB1 TCR. Ala mutagenesis was performed on residues Asp30 $\beta$  and Tyr31 $\beta$  in the CDR1 $\beta$  loop and residues Tyr57 $\beta$  and Val58 $\beta$  in the CDR2 $\beta$  loop (Fig. 4A and B). In addition, Tyr31 $\beta$  was mutated to Thr to mimic the CDR1 $\beta$  loop encoded by the five other *TRBV* genes that share Asp30 $\beta$  (Fig. 4A and B). Affinity values for each TCR mutant, measured by surface plasmon resonance (SPR), were compared with the affinity of the *wt* TCR. The results showed that mutations in the CDR2 $\beta$  loop exerted a moderate effect, decreasing binding affinity by 3-fold compared with the NB1 TCR (Fig. 4A and B). In contrast, mutation of Tyr31 $\beta$

to either Ala or Thr in the CDR1 $\beta$  loop substantially reduced binding to H-2D<sup>b</sup>-GAP50<sub>40-48</sub>, resulting in K<sub>d</sub><sub>eq</sub> values >200  $\mu$ M (Fig. 4A and B). As shown in Fig. 3I and Table S4, Tyr31 $\beta$  contacted both H-2D<sup>b</sup> and P8-Y. Additionally, mutation of Asp30 $\beta$  to Ala abolished binding to H-2D<sup>b</sup>-GAP50<sub>40-48</sub> (Fig. 4A and B). The Asp30 $\beta$  residue contacted the peptide alone via a salt bridge with P7-K, one of the two defined “hotspot” residues for TCR recognition (Fig. 3J and Table S4).

The unique germline-encoded CDR1 $\beta$  <sup>30</sup>DY<sup>31</sup> motif within the V $\beta$ 8.1 segment therefore underpinned both the extreme TCR bias and the residue-specific patterns of epitope recognition that characterized the CD8<sup>+</sup> T cell response to H-2D<sup>b</sup>-GAP50<sub>40-48</sub>.

### **The naive GAP50<sub>40-48</sub>-specific CD8<sup>+</sup> T cell repertoire is extraordinarily large**

Extreme TCR focusing described in the literature appears to result primarily from the selection of high-affinity clonotypes during repeated or persistent infection (Busch and Pamer, 1999; Malherbe et al., 2004; Price et al., 2005; Savage et al., 1999), but recombinatorial bias and structural constraints dictate the available pre-immune repertoire (Miles et al., 2011; Neller et al., 2015; Turner et al., 2006). We therefore adapted a tetramer-based enrichment protocol (Moon et al., 2007) to enumerate the naive repertoires specific for the *P. berghei* epitopes TRAP<sub>130-138</sub>, S20<sub>318-326</sub> and GAP50<sub>40-48</sub>. Parallel experiments were performed with tetramers representing epitopes derived from ovalbumin (H-2K<sup>b</sup>-OVA<sub>257-264</sub>) and lymphocytic choriomeningitis virus glycoprotein (H-2D<sup>b</sup>-LCMV GP<sub>33-41</sub>) to allow comparison with previously reported evaluations of the naive antigen-specific T cell repertoire (Jenkins and Moon, 2012).

Precursor numbers specific for OVA<sub>257-264</sub> and GP<sub>33-41</sub> were consistent with prior reports ( $183 \pm 33$  and  $358 \pm 40$  cells, respectively, Fig. 5A) (Jenkins and Moon, 2012). The naive S20<sub>318-326</sub>-specific repertoire was relatively small ( $\sim 79 \pm 19$  cells), while fewer than 10 cells were counted in the TRAP<sub>130-138</sub>-specific repertoire (Fig. 5A). In contrast, as described recently (Gordon et al., 2015), the GAP50<sub>40-48</sub>-specific naive repertoire was extraordinarily large ( $2,935 \pm 305$  cells, Fig. 5A). The upper limit for a naive antigen-specific CD8<sup>+</sup> T cell repertoire in mice was previously established at 1,200–1,500 cells for the MCMV M45<sub>985-993</sub> and VacV B8R<sub>20-27</sub> epitopes (Jenkins and Moon, 2012). The GAP50<sub>40-48</sub>-specific repertoire therefore constituted the largest naive

antigen-specific CD8<sup>+</sup> T cell pool yet described (Fig. 5B). Moreover, >99% of naive GAP50<sub>40-48</sub>-specific CD8<sup>+</sup> T cells expressed Vβ8.1 (Fig. 5A). These findings indicated that the extreme TCR Vβ bias observed in the memory CD8<sup>+</sup> T cell pool did not evolve as a consequence of repertoire focusing in response to antigenic challenge, but instead reflected intrinsic recognition of the GAP50<sub>40-48</sub> epitope characterized by absolute dependence on the interaction with Vβ8.1.

Phenotypically, the GAP50<sub>40-48</sub>-specific precursors resembled classical naive CD8<sup>+</sup> T cells, comprised of a large CD44<sup>lo</sup> population (>90%) and a small CD44<sup>hi</sup> “virtual memory” population (<10%) akin to OT-I and P14 TCR-Tg cells from naive mice (Fig. 5C) (Akue et al., 2012). Expression of the CD5 surface protein, which acts as a surrogate marker for the strength of TCR activation induced by self-derived MHCp complexes during thymic selection and frequently correlates with T cell avidity for antigen (Fulton et al., 2015; Mandl et al., 2013), was uniformly higher on naive GAP50<sub>40-48</sub>-specific CD8<sup>+</sup> T cells compared with the majority of non-GAP50<sub>40-48</sub>-specific naive CD8<sup>+</sup> T cells in the same host and mirrored levels expressed by OT-I cells, which express high-affinity TCRs (Fig. 5D) (Kedl et al., 2000). These data suggested that the extremely large pool of Vβ8.1<sup>+</sup> precursors specific for the GAP50<sub>40-48</sub> epitope arose as a consequence of strong thymic selection.

### **Absence of Vβ8.1 compromises the GAP50<sub>40-48</sub>-specific CD8<sup>+</sup> T cell response**

The results of our structural and mutagenesis studies indicated that immune responses to GAP50<sub>40-48</sub> required the presence of Vβ8.1. To test this hypothesis, we studied the generation of GAP50<sub>40-48</sub>-specific CD8<sup>+</sup> T cell responses in C57/L (H-2<sup>b</sup>) mice, which lack Vβ8 (Behlke et al., 1986). For this purpose, C57/L mice and control B6 mice were exposed to infection with 10<sup>3</sup> *P. berghei* ANKA sporozoites, a challenge that induces ECM in susceptible mouse strains.

In contrast to B6 mice, which generated GAP50<sub>40-48</sub>-specific responses comprising 4–5% of the total CD8<sup>+</sup> T cell pool in peripheral blood and >10% of the total CD8<sup>+</sup> T cell pool in the brain by day 7 post-infection, the GAP50<sub>40-48</sub>-specific response in C57/L mice was undetectable in both compartments (Fig. 6A and B). This finding strongly suggested that the GAP50<sub>40-48</sub>-specific CD8<sup>+</sup> T cell response was critically

dependent on  $V\beta 8.1$ . In addition, B6 x C57/L F1 mice mounted substantial  $V\beta 8.1^+$  GAP50<sub>40-48</sub>-specific CD8<sup>+</sup> T cell responses after infection with LM-GAP50<sub>40-48</sub> or *P. berghei* ANKA (data not shown), excluding negative selection of GAP50<sub>40-48</sub>-specific naive precursors in C57/L mice. However, C57/L mice lack other  $V\beta$  genes ( $V\beta 5$ ,  $V\beta 8$ ,  $V\beta 9$ ,  $V\beta 11$  and  $V\beta 12$ ) (Behlke et al., 1986), which could potentially compromise the ability to mount alternative responses to GAP50<sub>40-48</sub>. Countering this argument, the magnitude of the total *P. berghei*-specific CD8<sup>+</sup> T cell response, as detected by the frequency of CD8<sup>+</sup> T cells expressing surrogate activation markers (CD11a<sup>hi</sup> CD8<sup>lo</sup>) (Rai et al., 2009) at day 7 post-infection, was essentially identical in B6 and C57/L mice (Fig. 6C). Moreover, C57/L mice did not develop ECM, instead they survived beyond day 9 post-infection and succumbed to high-level parasitemia after ~3 weeks (Fig. 6D). Thus, the  $V\beta 8.1$  gene was necessary for the generation of detectable GAP50<sub>40-48</sub>-specific CD8<sup>+</sup> T cell responses and the development of ECM.

### **GAP50<sub>40-48</sub>-specific CD8<sup>+</sup> T cells are pathogenic in ECM**

A recent publication suggested that GAP50<sub>40-48</sub>-specific CD8<sup>+</sup> T cells play a key role in the pathogenesis of ECM in susceptible B6 mice (Howland et al., 2013). Mechanistically, accumulation of GAP50<sub>40-48</sub>-specific CD8<sup>+</sup> T cells in the brain could lead to eventual rupture of the blood-brain-barrier, which triggers well recognized neurological symptoms leading to rapid death (7–9 days post-infection) (Howland et al., 2013). In contrast to susceptible B6 mice, which all succumbed to ECM by day 7 post-infection with *P. berghei* ANKA-parasitized red blood cells (pRBCs), only 20% of CB6F1 mice succumbed to ECM (Fig. 6E). We therefore considered the possibility that a strain-specific difference in the size of the naive GAP50<sub>40-48</sub>-specific CD8<sup>+</sup> T cell repertoire might underlie these differential outcomes. Tetramer pull-down of naive GAP50<sub>40-48</sub>-specific CD8<sup>+</sup> T cells revealed that CB6F1 mice harbored ~3-fold fewer precursors than B6 mice (Fig. 6F). Moreover, this smaller naive pool resulted in a smaller GAP50<sub>40-48</sub>-specific CD8<sup>+</sup> T cell response in CB6F1 mice compared with B6 mice at day 6 post-infection with *P. berghei* ANKA pRBCs (Fig. 6G). These results suggested that a GAP50<sub>40-48</sub>-specific CD8<sup>+</sup> T cell response threshold might be required for the induction of ECM. To confirm a threshold-dependent pathogenic role for GAP50<sub>40-48</sub>-specific

CD8<sup>+</sup> T cells in ECM, we generated a large GAP50<sub>40-48</sub>-specific CD8<sup>+</sup> T cell response in CB6F1 or B6 mice prior to infection with *P. berghei* ANKA. We observed no meaningful difference in the onset of ECM symptoms or the mortality rate between previously immunized and non-immunized B6 mice, demonstrating that sufficient numbers of GAP50<sub>40-48</sub>-specific effector CD8<sup>+</sup> T cells can be generated from the large pool of naive precursors in this susceptible strain (Fig. 6H). In contrast, prior immunization against GAP50<sub>40-48</sub> was required to render all CB6F1 mice susceptible to ECM after *P. berghei* ANKA infection (Fig. 6I). Collectively, these findings demonstrated that a numerical threshold delimited the pathogenicity of GAP50<sub>40-48</sub>-specific CD8<sup>+</sup> T cells in the etiology of ECM.

### **GAP50<sub>40-48</sub>-specific CD8<sup>+</sup> T cells protect against LM-GAP50<sub>40-48</sub>**

Although pathogenic in the context of ECM, we hypothesized that the rapid generation of a substantial GAP50<sub>40-48</sub>-specific response from the large number of naive precursors may protect against infection controlled primarily by CD8<sup>+</sup> T cells. To address this possibility, we determined if B6 mice could better control primary infection with virulent LM-GAP50<sub>40-48</sub> compared with virulent *wt* LM.

To ensure comparability, we first established that the two different strains of LM exhibited similar virulence in the absence of a GAP50<sub>40-48</sub>-specific CD8<sup>+</sup> T cell response. For this purpose, we infected BALB/c mice (H-2<sup>d</sup>), which were non-responsive to the H-2D<sup>b</sup>-restricted GAP50<sub>40-48</sub> epitope (Fig. 7A). Bacterial burden assessed in the spleens of infected mice 5 days after infection with 5 x 10<sup>3</sup> colony-forming units (CFU) of each strain was similar between the two groups, suggesting equivalent virulence *in vivo* (Fig. 7B). In contrast, we measured ~10-fold fewer bacteria in the spleens of LM-GAP50<sub>40-48</sub>-infected B6 mice compared with *wt* LM-infected B6 mice (Fig. 7C–D). This superior control of bacterial infection in LM-GAP50<sub>40-48</sub>-infected B6 mice was accompanied by a large GAP50<sub>40-48</sub> specific response, comprising >8% of the total CD8<sup>+</sup> T cell pool in the spleen (Fig. 7E). The expansion of GAP50<sub>40-48</sub>-specific effector cells from a large pool of naive precursors therefore conferred protection in the context of an infection controlled by CD8<sup>+</sup> T cells.

## DISCUSSION

Conceptual frameworks developed in the 1970s, prior to a detailed understanding of the molecular interactions that govern T cell antigen recognition, established the notion of genetically controlled immune responsiveness. Overwhelming experimental data have since accumulated to validate one original proposition that MHC-linked *Ir* genes dictate the presentation of specific antigens in immunogenic form (Benacerraf and Germain, 1978). There is also some evidence to support the idea that germline-encoded components of the TCR interact preferentially with defined MHC allotypes (Garcia et al., 2009; Scott-Browne et al., 2009), building on the earlier theoretical work of Niels Jerne (Jerne, 1971). However, it has not been shown previously that heritable elements of an antigen receptor can license immune reactivity, a scenario postulated almost four decades ago as an alternative model to explain the *Ir* gene phenomenon (Benacerraf and Germain, 1978). In this study, we demonstrated that CD8<sup>+</sup> T cell responses specific for the murine malaria epitope GAP50<sub>40-48</sub> were entirely dependent on amino acid residues unique to the TCR V $\beta$ 8.1 segment, thereby providing insights into the genetic mechanisms that control adaptive immunity.

As a consequence of structural constraints focused primarily on the CDR1 $\beta$  loop, both naive and antigen-expanded H-2D<sup>b</sup>-restricted GAP50<sub>40-48</sub>-specific CD8<sup>+</sup> T cells almost invariably express V $\beta$ 8.1<sup>+</sup> TCRs. Similarly extreme biases are typically associated with innate-like responses to non-peptidic antigens presented by non-classical MHC molecules, although immune reactivity among these unconventional T cell subsets is generally endowed by a conserved TCR $\alpha$  chain (Van Rhijn et al., 2015). Narrow TCR repertoires specific for peptide epitopes have previously been linked with low numbers of naive precursors (Moon et al., 2007) and clonal selection during the genesis of memory populations, especially in the presence of constant or repetitive antigen stimulation (Busch and Pamer, 1999; Price et al., 2005; Savage et al., 1999). Paradoxically, the pre-immune GAP50<sub>40-48</sub>-specific repertoire was the largest yet described in mice, numbering ~3,000 cells in a naive B6 host. Moreover, this substantial precursor pool did not seem to arise as a consequence of expansion into the virtual memory subset (Haluszczak et al., 2009), as >90% of naive GAP50<sub>40-48</sub>-specific CD8<sup>+</sup> T cells expressed low levels of CD44 (Akue et al., 2012). Although the self-derived

peptides associated with positive selection of these antigen-specific precursors remain unknown, the uniformly high expression of CD5 by naive GAP50<sub>40-48</sub>-specific CD8<sup>+</sup> T cells suggested the existence of strong TCR-mediated interactions in the thymus (Mandl et al., 2013). It is also notable that *Vβ8* gene segments are highly represented in laboratory mouse strains (Wilson et al., 2001). High numbers of naive GAP50<sub>40-48</sub>-specific CD8<sup>+</sup> T cells therefore most likely emerged as a consequence of both permissive thymic selection and the frequent generation of *Vβ8.1*<sup>+</sup> transcripts during the process of somatic recombination. In addition, the presence of a highly conserved *Vβ-Dβ* junction lacking N additions suggested that convergent gene rearrangements, which occur more commonly on a probabilistic basis (Quigley et al., 2010), effectively licensed the extreme penetrance of the *Vβ8.1* gene-encoded phenotype.

So what are the immunological consequences of such a large pool of antigen-specific precursors in the naive CD8<sup>+</sup> T cell compartment? Earlier work indicated that CD8<sup>+</sup> T cells expressing *Vβ8.1/Vβ8.2*<sup>+</sup> TCRs are highly prevalent during malaria infection and contribute to the pathogenesis of ECM (Mariotti-Ferrandiz et al., 2016). In addition, it had been shown previously that high-dose tolerization with the GAP50<sub>40-48</sub> peptide abrogates disease susceptibility in B6 mice (Howland et al., 2013). These observations can be explained by our finding that an extremely large pool of *Vβ8.1*<sup>+</sup> antigen-specific naive precursors (~3,000 cells) underpinned the immunodominant CD8<sup>+</sup> T cell response to GAP50<sub>40-48</sub> and the susceptibility of B6 mice to ECM. In contrast, CB6F1 mice harbored a diminished pool of antigen-specific naïve precursors (~1,000 cells), leading to smaller GAP50<sub>40-48</sub>-specific CD8<sup>+</sup> T cell responses and relative resistance to ECM. This causal association was confirmed by the observation that increasing the number of GAP50<sub>40-48</sub>-specific CD8<sup>+</sup> T cells in CB6F1 mice prior to infection rendered them susceptible to ECM. It remains unclear if similar germline biases can dictate immune responses to malarial antigens in humans, but our data nonetheless provide proof-of-concept that genetic associations with disease outcome can be extended to loci encoding components of the TCR. Moreover, the peak incidence of severe anemia during malaria infection occurs in children under 2 years of age, while cerebral malaria occurs most commonly in children aged 3–5 years who have prior exposure to infection (Struik and Riley, 2004). These epidemiological



patterns are consistent with the possibility that larger pre-infection repertoires of malarial antigen-specific T cells predispose to the development of cerebral malaria.

GAP50<sub>40-48</sub>-specific memory CD8<sup>+</sup> T cells are not protective during the liver-stage of murine malaria (Doll et al., 2016; Horne-Debets et al., 2016; van der Heyde et al., 1993; Vinetz et al., 1990), and the capacity of CD8<sup>+</sup> T cells to protect during blood-stage malaria remains controversial (Horne-Debets et al., 2016; Imai et al., 2010; van der Heyde et al., 1993; Vinetz et al., 1990). Thus, the pathogenic effects of GAP50<sub>40-48</sub>-specific CD8<sup>+</sup> T cells in ECM most likely resulted from a large population of precursors, which expanded rapidly after infection to generate substantial numbers of effector cells, leading to sustained immune activation without elimination of the pathogen. In contrast, rapid expansion from the same population of precursors enhanced immune control of primary infection with *L. monocytogenes* expressing the GAP50<sub>40-48</sub> epitope. An unusually large naive CD8<sup>+</sup> T cell pool can therefore be pathogenic or protective, depending on the nature of the infectious challenge.

In conclusion, our data provide direct evidence that a germline-encoded TCR segment can determine immune responsiveness to an exogenous peptide antigen, thereby extending the concept of *Ir* genes beyond the MHC. The unique features associated with this phenomenon may allow novel interventions to improve vaccine efficacy and limit immune pathology in humans, pending further studies to identify similar genetic associations between disease outcome and heritable components of the TCR.

## **AUTHOR CONTRIBUTIONS**

NVBB, SG, KL, TMJ, LP, SLU, CF, DAP, JR and JTH designed the study. NVBB, SG, KL, TMJ, LP, SLU, KLM and CF conducted experiments. NVBB, SG, KL, TMJ, LP, SLU, KLM, CF, DAP, JR and JTH analyzed data and interpreted results. NVBB and SG drafted the manuscript. NVBB, SG, KL, TMJ, LP, SLU, CF, DAP, JR and JTH edited the manuscript.

## **ACKNOWLEDGEMENTS**

We thank Marc Jenkins for helpful discussions, Vladimir Badovinac and Stanley Perlman for constructive comments on the manuscript, Lisa Hancox and Steven Moieffer for excellent technical support, and staff at the New York University Insectary Core and the University of Iowa Flow Cytometry Core. This work was supported by grants from the National Institutes of Health (NIH) to JTH (AI42767, AI85515, AI95178 and AI100527), the Australian Research Council (ARC) and the Australian National Health and Medical Research Council (NHMRC) to JR, and the Wellcome Trust to DAP (100326/Z/12/Z). NVBB was supported by NIH grant T32 AI007511, and SLU was supported by NIH grant T32 AI007343. SG is a Monash Senior Research Fellow, DAP is a Wellcome Trust Senior Investigator, and JR is an ARC Australian Laureate Fellow.

## REFERENCES

- Akue, A.D., Lee, J.Y., and Jameson, S.C. (2012). Derivation and maintenance of virtual memory CD8 T cells. *J Immunol* 188, 2516-2523.
- Amani, V., Vigario, A.M., Belnoue, E., Marussig, M., Fonseca, L., Mazier, D., and Renia, L. (2000). Involvement of IFN-gamma receptor-mediated signaling in pathology and anti-malarial immunity induced by *Plasmodium berghei* infection. *Eur J Immunol* 30, 1646-1655.
- Badovinac, V.P., and Harty, J.T. (2000). Adaptive immunity and enhanced CD8+ T cell response to *Listeria monocytogenes* in the absence of perforin and IFN-gamma. *J Immunol* 164, 6444-6452.
- Badovinac, V.P., Messingham, K.A., Jabbari, A., Haring, J.S., and Harty, J.T. (2005). Accelerated CD8+ T-cell memory and prime-boost response after dendritic-cell vaccination. *Nat Med* 11, 748-756.
- Behlke, M.A., Chou, H.S., Huppi, K., and Loh, D.Y. (1986). Murine T-cell receptor mutants with deletions of beta-chain variable region genes. *PNAS* 83, 767-771.
- Benacerraf, B. (1974). Editorial: Immune response genes. *Scand J Immunol* 3, 381-386.
- Benacerraf, B., and Germain, R.N. (1978). The immune response genes of the major histocompatibility complex. *Immunol Rev* 38, 70-119.
- Benacerraf, B., and McDevitt, H.O. (1972). Histocompatibility-linked immune response genes. *Science* 175, 273-279.
- Bendelac, A., Rivera, M.N., Park, S.H., and Roark, J.H. (1997). Mouse CD1-specific NK1 T cells: development, specificity, and function. *Annu Rev Immunol* 15, 535-562.
- Bettini, M.L., Bettini, M., Nakayama, M., Guy, C.S., and Vignali, D.A. (2013). Generation of T cell receptor-retrogenic mice: improved retroviral-mediated stem cell gene transfer. *Nat Protoc* 8, 1837-1840.
- Blattman, J.N., Antia, R., Sourdive, D.J., Wang, X., Kaech, S.M., Murali-Krishna, K., Altman, J.D., and Ahmed, R. (2002). Estimating the precursor frequency of naive antigen-specific CD8 T cells. *J Exp Med* 195, 657-664.
- Boubou, M.I., Collette, A., Voegtli, D., Mazier, D., Cazenave, P.A., and Pied, S. (1999). T cell response in malaria pathogenesis: selective increase in T cells carrying the TCR V(beta)8 during experimental cerebral malaria. *Int Immunol* 11, 1553-1562.
- Brewster, D.R., Kwiatkowski, D., and White, N.J. (1990). Neurological sequelae of cerebral malaria in children. *Lancet* 336, 1039-1043.

Busch, D.H., and Pamer, E.G. (1999). T cell affinity maturation by selective expansion during infection. *J Exp Med* 189, 701-710.

Busch, D.H., Pilip, I., and Pamer, E.G. (1998). Evolution of a complex T cell receptor repertoire during primary and recall bacterial infection. *J Exp Med* 188, 61-70.

Cabaniols, J.P., Fazilleau, N., Casrouge, A., Kourilsky, P., and Kanellopoulos, J.M. (2001). Most alpha/beta T cell receptor diversity is due to terminal deoxynucleotidyl transferase. *J Exp Med* 194, 1385-1390.

Chothia, C., Boswell, D.R., and Lesk, A.M. (1988). The outline structure of the T-cell alpha beta receptor. *EMBO J* 7, 3745-3755.

Collaborative Computational Project, Number 4 (1994). The CCP4 suite: programs for protein crystallography. *Acta Crystallogr D Biol Crystallogr* 50, 760-763.

Dai, S., Huseby, E.S., Rubtsova, K., Scott-Browne, J., Crawford, F., Macdonald, W.A., Marrack, P., and Kappler, J.W. (2008). Crossreactive T cells spotlight the germline rules for alphabeta T cell-receptor interactions with MHC molecules. *Immunity* 28, 324-334.

Davis, M.M., and Bjorkman, P.J. (1988). T-cell antigen receptor genes and T-cell recognition. *Nature* 334, 395-402.

Davis, M.M., Krogsgaard, M., Huppa, J.B., Sumen, C., Purbhoo, M.A., Irvine, D.J., Wu, L.C., and Ehrlich, L. (2003). Dynamics of cell surface molecules during T cell recognition. *Annu Rev Biochem* 72, 717-742.

Day, E.B., Guillonneau, C., Gras, S., La Gruta, N.L., Vignali, D.A., Doherty, P.C., Purcell, A.W., Rossjohn, J., and Turner, S.J. (2011). Structural basis for enabling T-cell receptor diversity within biased virus-specific CD8<sup>+</sup> T-cell responses. *PNAS* 108, 9536-9541.

DeLano, W.L. (2002). The PyMOL Molecular Graphics System. <http://www.pymol.org>.

Doll, K.L., Pewe, L.L., Kurup, S.P., and Harty, J.T. (2016). Discriminating Protective from Nonprotective Plasmodium-Specific CD8<sup>+</sup> T Cell Responses. *J Immunol* 196, 4253-4262.

Emsley, P., and Cowtan, K. (2004). Coot: model-building tools for molecular graphics. *Acta Crystallogr D Biol Crystallogr* 60, 2126-2132.

Engwerda, C., Belnoue, E., Gruner, A.C., and Renia, L. (2005). Experimental models of cerebral malaria. *Curr Top Microbiol Immunol* 297, 103-143.

Evans, P. (2006). Scaling and assessment of data quality. *Acta Crystallogr D Biol Crystallogr* 62, 72-82.

Fulton, R.B., Hamilton, S.E., Xing, Y., Best, J.A., Goldrath, A.W., Hogquist, K.A., and Jameson, S.C. (2015). The TCR's sensitivity to self peptide-MHC dictates the ability of naive CD8(+) T cells to respond to foreign antigens. *Nat Immunol* 16, 107-117.

Garcia, K.C., Adams, J.J., Feng, D., and Ely, L.K. (2009). The molecular basis of TCR germline bias for MHC is surprisingly simple. *Nat Immunol* 10, 143-147.

Godfrey, D.I., Uldrich, A.P., McCluskey, J., Rossjohn, J., and Moody, D.B. (2015). The burgeoning family of unconventional T cells. *Nat Immunol* 16, 1114-1123.

Goldrath, A.W., and Bevan, M.J. (1999). Selecting and maintaining a diverse T-cell repertoire. *Nature* 402, 255-262.

Gordon, E.B., Hart, G.T., Tran, T.M., Waisberg, M., Akkaya, M., Kim, A.S., Hamilton, S.E., Pena, M., Yazew, T., Qi, C.F., *et al.* (2015). Targeting glutamine metabolism rescues mice from late-stage cerebral malaria. *PNAS* 112, 13075-13080.

Gras, S., Burrows, S.R., Kjer-Nielsen, L., Clements, C.S., Liu, Y.C., Sullivan, L.C., Bell, M.J., Brooks, A.G., Purcell, A.W., McCluskey, J., and Rossjohn, J. (2009). The shaping of T cell receptor recognition by self-tolerance. *Immunity* 30, 193-203.

Hafalla, J.C., Bauza, K., Friesen, J., Gonzalez-Aseguinolaza, G., Hill, A.V., and Matuschewski, K. (2013). Identification of targets of CD8(+) T cell responses to malaria liver stages by genome-wide epitope profiling. *PLoS Pathog* 9, e1003303.

Haluszczak, C., Akue, A.D., Hamilton, S.E., Johnson, L.D., Pujanauski, L., Teodorovic, L., Jameson, S.C., and Kedl, R.M. (2009). The antigen-specific CD8+ T cell repertoire in unimmunized mice includes memory phenotype cells bearing markers of homeostatic expansion. *J Exp Med* 206, 435-448.

Haque, A., Best, S.E., Unosson, K., Amante, F.H., de Labastida, F., Anstey, N.M., Karupiah, G., Smyth, M.J., Heath, W.R., and Engwerda, C.R. (2011). Granzyme B expression by CD8+ T cells is required for the development of experimental cerebral malaria. *J Immunol* 186, 6148-6156.

Holst, J., Szymczak-Workman, A.L., Vignali, K.M., Burton, A.R., Workman, C.J., and Vignali, D.A. (2006). Generation of T-cell receptor retrogenic mice. *Nat Protoc* 1, 406-417.

Horne-Debets, J.M., Karunaratne, D.S., Faleiro, R.J., Poh, C.M., Renia, L., and Wykes, M.N. (2016). Mice lacking Programmed cell death-1 show a role for CD8(+) T cells in long-term immunity against blood-stage malaria. *Sci Rep* 6, 26210.

Howland, S.W., Poh, C.M., Gun, S.Y., Claser, C., Malleret, B., Shastri, N., Ginhoux, F., Grotenbreg, G.M., and Renia, L. (2013). Brain microvessel cross-presentation is a hallmark of experimental cerebral malaria. *EMBO Mol Med* 5, 916-931.

Imai, T., Shen, J., Chou, B., Duan, X., Tu, L., Tetsutani, K., Moriya, C., Ishida, H., Hamano, S., Shimokawa, C., *et al.* (2010). Involvement of CD8<sup>+</sup> T cells in protective immunity against murine blood-stage infection with *Plasmodium yoelii* 17XL strain. *Eur J Immunol* 40, 1053-1061.

Jenkins, M.K., and Moon, J.J. (2012). The role of naive T cell precursor frequency and recruitment in dictating immune response magnitude. *J Immunol* 188, 4135-4140.

Jerne, N.K. (1971). The somatic generation of immune recognition. *Eur J Immunol* 1, 1-9.

Kabsch, W. (2010). XDS. *Acta Crystallogr D Biol Crystallogr* 66, 125-132.

Kedl, R.M., Rees, W.A., Hildeman, D.A., Schaefer, B., Mitchell, T., Kappler, J., and Marrack, P. (2000). T cells compete for access to antigen-bearing antigen-presenting cells. *J Exp Med* 192, 1105-1113.

Kjer-Nielsen, L., Clements, C.S., Brooks, A.G., Purcell, A.W., McCluskey, J., and Rossjohn, J. (2002). The 1.5 Å crystal structure of a highly selected antiviral T cell receptor provides evidence for a structural basis of immunodominance. *Structure* 10, 1521-1532.

Lefranc, M.P. (2003). IMGT databases, web resources and tools for immunoglobulin and T cell receptor sequence analysis, <http://imgt.cines.fr>. *Leukemia* 17, 260-266.

Mach, N., Gillessen, S., Wilson, S.B., Sheehan, C., Mihm, M., and Dranoff, G. (2000). Differences in dendritic cells stimulated in vivo by tumors engineered to secrete granulocyte-macrophage colony-stimulating factor or Flt3-ligand. *Cancer Res* 60, 3239-3246.

Malherbe, L., Hausl, C., Teyton, L., and McHeyzer-Williams, M.G. (2004). Clonal selection of helper T cells is determined by an affinity threshold with no further skewing of TCR binding properties. *Immunity* 21, 669-679.

Mandl, J.N., Monteiro, J.P., Vrisekoop, N., and Germain, R.N. (2013). T cell-positive selection uses self-ligand binding strength to optimize repertoire recognition of foreign antigens. *Immunity* 38, 263-274.

Mariotti-Ferrandiz, E., Pham, H.P., Dulauroy, S., Gorgette, O., Klatzmann, D., Cazenave, P.A., Pied, S., and Six, A. (2016). A TCRbeta Repertoire Signature Can Predict Experimental Cerebral Malaria. *PLoS One* 11, e0147871.

Marshak, A., Doherty, P.C., and Wilson, D.B. (1977). The control of specificity of cytotoxic T lymphocytes by the major histocompatibility complex (AG-B) in rats and identification of a new alloantigen system showing no AG-B restriction. *J Exp Med* 146, 1773-1790.

McDevitt, H.O., and Chinitz, A. (1969). Genetic control of the antibody response: relationship between immune response and histocompatibility (H-2) type. *Science* 163, 1207-1208.

Miles, J.J., Douek, D.C., and Price, D.A. (2011). Bias in the alphabeta T-cell repertoire: implications for disease pathogenesis and vaccination. *Immunol Cell Biol* 89, 375-387.

Moon, J.J., Chu, H.H., Pepper, M., McSorley, S.J., Jameson, S.C., Kedl, R.M., and Jenkins, M.K. (2007). Naive CD4(+) T cell frequency varies for different epitopes and predicts repertoire diversity and response magnitude. *Immunity* 27, 203-213.

Neller, M.A., Ladell, K., McLaren, J.E., Matthews, K.K., Gostick, E., Pentier, J.M., Dolton, G., Schauenburg, A.J., Koning, D., Fontaine Costa, A.I., *et al.* (2015). Naive CD8(+) T-cell precursors display structured TCR repertoires and composite antigen-driven selection dynamics. *Immunol Cell Biol* 93, 625-633.

Obar, J.J., Khanna, K.M., and Lefrancois, L. (2008). Endogenous naive CD8+ T cell precursor frequency regulates primary and memory responses to infection. *Immunity* 28, 859-869.

Owens, T., and Zeine, R. (1989). The cell biology of T-dependent B cell activation. *Biochem Cell Biol* 67, 481-489.

Pham, N.L., Badovinac, V.P., and Harty, J.T. (2009). A default pathway of memory CD8 T cell differentiation after dendritic cell immunization is deflected by encounter with inflammatory cytokines during antigen-driven proliferation. *J Immunol* 183, 2337-2348.

Price, D.A., Brenchley, J.M., Ruff, L.E., Betts, M.R., Hill, B.J., Roederer, M., Koup, R.A., Migueles, S.A., Gostick, E., Wooldridge, L., *et al.* (2005). Avidity for antigen shapes clonal dominance in CD8+ T cell populations specific for persistent DNA viruses. *J Exp Med* 202, 1349-1361.

Quigley, M.F., Almeida, J.R., Price, D.A., and Douek, D.C. (2011). Unbiased molecular analysis of T cell receptor expression using template-switch anchored RT-PCR. *Curr Protoc Immunol Chapter 10*, Unit10 33.

Quigley, M.F., Greenaway, H.Y., Venturi, V., Lindsay, R., Quinn, K.M., Seder, R.A., Douek, D.C., Davenport, M.P., and Price, D.A. (2010). Convergent recombination shapes the clonotypic landscape of the naive T-cell repertoire. *PNAS* 107, 19414-19419.

Rai, D., Pham, N.L., Harty, J.T., and Badovinac, V.P. (2009). Tracking the total CD8 T cell response to infection reveals substantial discordance in magnitude and kinetics between inbred and outbred hosts. *J Immunol* 183, 7672-7681.

Read, R.J. (2001). Pushing the boundaries of molecular replacement with maximum likelihood. *Acta Crystallogr D Biol Crystallogr* 57, 1373-1382.

Rossjohn, J., Gras, S., Miles, J.J., Turner, S.J., Godfrey, D.I., and McCluskey, J. (2015). T cell antigen receptor recognition of antigen-presenting molecules. *Annu Rev Immunol* 33, 169-200.

Savage, P.A., Boniface, J.J., and Davis, M.M. (1999). A kinetic basis for T cell receptor repertoire selection during an immune response. *Immunity* 10, 485-492.

Scott-Browne, J.P., White, J., Kappler, J.W., Gapin, L., and Marrack, P. (2009). Germline-encoded amino acids in the alphabeta T-cell receptor control thymic selection. *Nature* 458, 1043-1046.

Struik, S.S., and Riley, E.M. (2004). Does malaria suffer from lack of memory? *Immunol Rev* 201, 268-290.

Townsend, A.R., Gotch, F.M., and Davey, J. (1985). Cytotoxic T cells recognize fragments of the influenza nucleoprotein. *Cell* 42, 457-467.

Turner, S.J., Doherty, P.C., McCluskey, J., and Rossjohn, J. (2006). Structural determinants of T-cell receptor bias in immunity. *Nat Rev Immunol* 6, 883-894.

Valkenburg, S.A., Quinones-Parra, S., Gras, S., Komadina, N., McVernon, J., Wang, Z., Halim, H., Iannello, P., Cole, C., Laurie, K., *et al.* (2013). Acute emergence and reversion of influenza A virus quasiespecies within CD8<sup>+</sup> T cell antigenic peptides. *Nat Commun* 4, 2663.

van der Heyde, H.C., Manning, D.D., Roopenian, D.C., and Weidanz, W.P. (1993). Resolution of blood-stage malarial infections in CD8<sup>+</sup> cell-deficient beta 2-m0/0 mice. *J Immunol* 151, 3187-3191.

van der Merwe, P.A., and Dushek, O. (2011). Mechanisms for T cell receptor triggering. *Nat Rev Immunol* 11, 47-55.

Van Rhijn, I., Godfrey, D.I., Rossjohn, J., and Moody, D.B. (2015). Lipid and small-molecule display by CD1 and MR1. *Nat Rev Immunol* 15, 643-654.

Vinetz, J.M., Kumar, S., Good, M.F., Fowlkes, B.J., Berzofsky, J.A., and Miller, L.H. (1990). Adoptive transfer of CD8<sup>+</sup> T cells from immune animals does not transfer immunity to blood stage *Plasmodium yoelii* malaria. *J Immunol* 144, 1069-1074.



Wilson, A., Marechal, C., and MacDonald, H.R. (2001). Biased V beta usage in immature thymocytes is independent of DJ beta proximity and pT alpha pairing. *J Immunol* 166, 51-57.

Yanez, D.M., Manning, D.D., Cooley, A.J., Weidanz, W.P., and van der Heyde, H.C. (1996). Participation of lymphocyte subpopulations in the pathogenesis of experimental murine cerebral malaria. *J Immunol* 157, 1620-1624.

Young, A.C., Zhang, W., Sacchettini, J.C., and Nathenson, S.G. (1994). The three-dimensional structure of H-2Db at 2.4 Å resolution: implications for antigen-determinant selection. *Cell* 76, 39-50.

Zhao, J., Zhao, J., and Perlman, S. (2009). De novo recruitment of antigen-experienced and naive T cells contributes to the long-term maintenance of antiviral T cell populations in the persistently infected central nervous system. *J Immunol* 183, 5163-5170.

Zinkernagel, R.M. (1978). Thymus and lymphohemopoietic cells: their role in T cell maturation in selection of T cells' H-2-restriction-specificity and in H-2 linked Ir gene control. *Immunol Rev* 42, 224-270.

## FIGURE LEGENDS

### Figure 1: GAP50<sub>40-48</sub>-specific CD8<sup>+</sup> T cells express biased TCRs

(A, B) Mice were primed with peptide-coated DCs and boosted on day 7 with recombinant *L. monocytogenes* expressing the same epitope. (A) The TCR V $\beta$  repertoire was assessed using splenocytes isolated from immunized mice by staining with the indicated tetramers and V $\beta$ -specific antibodies. Results are shown for two mice for each antigen specificity. Data represent four independent experiments (n = 5 mice/group). Cumulative data are shown in Supplementary Figure 1B. (B) Extreme focusing of the GAP50<sub>40-48</sub>-specific repertoire does not reflect the overall frequency of V $\beta$ 8.1/8.2<sup>+</sup> clonotypes in the CD8<sup>+</sup> T cell compartment. Data represent three independent experiments (n = 4–5 mice/group). (C, D) Confirmation of TCR bias at the transcriptional level. Sequences were derived from GAP50<sub>40-48</sub>-specific CD8<sup>+</sup> T cells isolated from the spleens of mice previously immunized with DC-LM-GAP50<sub>40-48</sub> (total = 316 molecular clones). (C) Population-level analysis revealed an extreme bias towards V $\beta$ 8.1. (D) TCR V $\alpha$  sequence distributions from three different mice are depicted. No obvious bias was apparent in the V $\alpha$  repertoire. (E) Origin of CDR3 $\beta$  amino acids expressed relative to the total number of molecular V $\beta$ 8.1<sup>+</sup> clones (n = 5 mice). V $\beta$ : red; D $\beta$ : green; J $\beta$ : purple; N segments: white. (See also Figures S1–S3 and Table S1).

### Figure 2: TCR interactions focus on the C-terminal region of the GAP50<sub>40-48</sub> peptide

(A) The structure of the GAP50<sub>40-48</sub> peptide in complex with H-2D<sup>b</sup>. The GAP50<sub>40-48</sub> peptide is represented as black sticks in the antigen-binding cleft of H-2D<sup>b</sup> (white cartoon). The P2-Q and P9-L anchor residues are buried within the antigen-binding cleft, and P5-N acts as a secondary anchor residue forming hydrogen bonds (black dashes) with Gln97 (white stick) at the base of the antigen-binding cleft of H-2D<sup>b</sup> (white cartoon). (B) A panel of peptide mutants was generated by replacing amino acids with Ala or Ser at selected positions (red). Anchor residues are underlined. (C) Splenocytes isolated from GAP50<sub>40-48</sub>-immunized mice were restimulated for 5 h *in vitro* using *wt* or mutant peptides. The production of IFN $\gamma$  induced by stimulation with the different mutant

peptides is expressed relative to the production of IFN $\gamma$  induced by stimulation with the *wt* peptide. Data represent two independent experiments performed in triplicate. Bars represent mean  $\pm$  SD. Significance was assessed using a one-way ANOVA (\*\*\*\* $p < 0.0001$ ). (D) The effect of peptide substitutions on recognition of the H-2D<sup>b</sup>-GAP50<sub>40-48</sub> complex by specific CD8<sup>+</sup> T cell clones. The surface of H-2D<sup>b</sup> is shown in white. Peptide residues that were not mutated or did not affect IFN $\gamma$  production are shown in gray. Green represents up to a 25% decrease in T cell activation; orange represents up to a 70% decrease in T cell activation; red represents a total abrogation of T cell activation. (See also Figure S4 and Table S2).

### Figure 3: GAP50<sub>40-48</sub>-specific TCR bias is peptide-driven

(A) The crystal structure of the NB1 TCR ( $\alpha$  chain: pink cartoon;  $\beta$  chain: purple cartoon) bound to the GAP50<sub>40-48</sub> peptide (black sticks) presented by H-2D<sup>b</sup> (heavy chain: white cartoon;  $\beta$ 2m, wheat cartoon). (B) The CDR loop contribution to the BSA is represented as teal (CDR1 $\alpha$ ), green (CDR2 $\alpha$ ), purple (CDR3 $\alpha$ ), red (CDR1 $\beta$ ), orange (CDR2 $\beta$ ) or yellow (CDR3 $\beta$ ). Black spheres represent the center of mass for the V $\alpha$  and V $\beta$ . (C–E) The contribution (%) of the CDR loops to the interaction with H-2D<sup>b</sup>-GAP50<sub>40-48</sub> (C), GAP50<sub>40-48</sub> (D) and H-2D<sup>b</sup> (E). (F–K) Contact residues between H-2D<sup>b</sup>-GAP50<sub>40-48</sub> and CDR1 $\alpha$  (F), CDR2 $\alpha$  (G), CDR3 $\alpha$  (H), CDR1 $\beta$  (I, J), CDR2 $\beta$  (J) and CDR3 $\beta$  (K). The CDR color scheme is maintained though panels F–K. Residues that make contacts with the GAP50<sub>40-48</sub> peptide or H-2D<sup>b</sup> (white) are depicted as black and white sticks, respectively. The H-2D<sup>b</sup> molecule is represented as white cartoon, and hydrogen bonds are shown as black dashes. (See also Figure S5 and Tables S2–S5).

### Figure 4: Binding affinities of NB1 TCR mutants for H-2D<sup>b</sup>-GAP50<sub>40-48</sub>

(A) Surface plasmon resonance (SPR) analysis of NB1 *wt* (black) and the indicated mutant (colored) TCRs across a range of H-2D<sup>b</sup>-GAP50<sub>40-48</sub> concentrations up to a maximum of 200  $\mu$ M. Representative SPR binding curves are shown for the NB1 *wt* TCR (black) and NB1 mutant TCRs with the following  $\beta$  chain substitutions: Y31A (green), D30A (red), Y57A (pink), V58A (orange) and Y31A (blue). Each NB1 mutant TCR was tested in parallel with the NB1 *wt* TCR. (B) Summary table representing

equilibrium binding affinities of NB1 TCR mutants for H-2D<sup>b</sup>-GAP50<sub>40-48</sub>. NB: no binding; RU: response units. Data represent two independent experiments performed in duplicate (mean ± SEM). (See also Tables S6A and S6B).

**Figure 5: The naive GAP50<sub>40-48</sub>-specific CD8<sup>+</sup> T cell repertoire is extremely large**

(A) CD8<sup>+</sup> T cells specific for OVA<sub>257-264</sub>, GP<sub>33-41</sub>, GAP50<sub>40-48</sub>, S20<sub>318-326</sub> and TRAP<sub>130-138</sub> were enriched from the spleens and macroscopic lymph nodes of naive C57Bl/6 mice and used to calculate the final numbers of tetramer<sup>+</sup> cells indicated in each plot. Target cells were identified as CD8<sup>+</sup> CD90.2<sup>+</sup> CD11b<sup>-</sup> CD11c<sup>-</sup> B220<sup>-</sup> tetramer(APC)<sup>+</sup> tetramer(PE)<sup>+</sup>. Depicted numbers of naive precursors were calculated as mean ± SD from 11 mice for the GAP50<sub>40-48</sub>-specific repertoire. Right panel: Vβ8.1/8.2 expression on naive GAP50<sub>40-48</sub>-specific CD8<sup>+</sup> T cells. (B) Sizes of the naive repertoires specific for various CD8<sup>+</sup> T cell epitopes. The number of naive GAP50<sub>40-48</sub>-specific precursors is represented as a range from 2,700–3,250 cells (total n = 11 mice). (C, D) Phenotypic characterization of naive GAP50<sub>40-48</sub>-specific CD8<sup>+</sup> T cells. (C) Expression of CD44 on naive GAP50<sub>40-48</sub>-specific CD8<sup>+</sup> T cells was compared with CD8<sup>+</sup> T cells obtained from naive Tg OT-I and P14 mice. (D) Expression of CD5 on naive GAP50<sub>40-48</sub>-specific CD8<sup>+</sup> T cells was compared with total naive, non-GAP50<sub>40-48</sub>-specific CD8<sup>+</sup> T cells (left panel) and with naive Tg OT-I cells (right panel). Data represent two independent experiments (n = 4 mice/group). Bars depict mean ± SD.

**Figure 6: Vβ8.1 is required for the generation of GAP50<sub>40-48</sub>-specific CD8<sup>+</sup> T cells and the development of ECM**

(A, B) C57Bl/6 and C57/L mice were infected with 1,000 *P. berghei* ANKA sporozoites. H-2D<sup>b</sup>-GAP50<sub>40-48</sub> tetramer<sup>+</sup> cells were quantified in the blood (A) and brains (B) at day 7 post-infection (representative plots: left; summary graph: right). (C) Magnitude of the activated CD8<sup>+</sup> T cell response at day 7 post-infection, expressed as % CD11a<sup>hi</sup> CD8<sup>lo</sup> of total CD8<sup>+</sup> T cells (representative plots: left; summary graph: right). Naive control values were subtracted from individual values. Data represent two independent experiments (n = 3 mice/group). Bars depict mean ± SD. Significance was assessed using an unpaired, two-tailed t test (\*\*p < 0.01, \*\*\*p < 0.001). (D) Survival curves for

C57Bl/6 mice and C57/L mice after infection with *P. berghei* ANKA. Data represent three independent experiments (n = 5 mice/group). Significance was assessed using the Mantel-Cox log rank test (\*\*\*p = 0.001). (E) C57Bl/6 and CB6F1 mice were infected with  $10^6$  *P. berghei*-parasitized red blood cells (pRBCs). Mice were monitored for the development of ECM symptoms and scored for survival over a period of two weeks. Data represent three independent experiments (n = 5 mice/group). Significance was assessed using the Mantel-Cox log rank test (\*\*p = 0.0025). (F) GAP50<sub>40-48</sub>-specific CD8<sup>+</sup> T cells were tetramer-enriched from naive C57Bl/6 and CB6F1 mice and quantified to estimate repertoire size. Cumulative results are shown from two independent experiments (total n = 4 mice/group). Bars depict mean  $\pm$  SEM. Significance was assessed using an unpaired, two-tailed t test (\*\*\*\*p < 0.0001). (G) C57Bl/6 and CB6F1 mice were infected with  $10^6$  pRBCs. The GAP50<sub>40-48</sub>-specific CD8<sup>+</sup> T cell response was followed in the blood of infected mice using H-2D<sup>b</sup>-GAP50<sub>40-48</sub> tetramers. All C57Bl/6 mice succumbed to ECM by days 6 and 7, while all CB6F1 mice survived. Data represent two independent experiments (n = 5 mice/group). Bars depict mean  $\pm$  SD. Significance was assessed using an unpaired, two-tailed t test (\*\*\*\*p < 0.0001). (H, I) C57Bl/6 and CB6F1 mice were injected IV with  $5 \times 10^5$  GAP50<sub>40-48</sub> peptide-coated DCs and then infected 7 days later with recombinant attenuated LM-GAP50<sub>40-48</sub>. At a memory time point after LM infection, DC-LM-GAP50<sub>40-48</sub>-immunized or non-immunized mice were infected with  $10^6$  pRBCs. Survival curves are shown for C57Bl/6 mice (H) and CB6F1 mice (I). Data represent two independent experiments (n = 5 mice/group). Significance was assessed using the Mantel-Cox log rank test (p = 0.0993 in panel D; \*\*p = 0.0018 in panel E).

**Figure 7: Large numbers of GAP50<sub>40-48</sub>-specific CD8<sup>+</sup> T cells control primary *L. monocytogenes* infection**

(A) BALB/c mice were infected IV with  $5 \times 10^3$  CFU of *wt* LM or recombinant LM-GAP50<sub>40-48</sub>. Bacterial burden was measured in the spleen on day 5. Data represent two independent experiments (n = 4 mice/group). Bars depict mean  $\pm$  SD. (B) C57Bl/6 mice were infected IV with  $10^4$  CFU of *wt* LM or recombinant LM-GAP50<sub>40-48</sub>. Bacterial burden was measured in the spleen on day 5. Cumulative results are shown from three

independent experiments (total n = 14–15 mice/group). Bars depict mean  $\pm$  SEM. Significance was assessed using an unpaired, two-tailed t test (\*\*\*\*p<0.0001). (C) Representative flow cytometry plots showing H-2D<sup>b</sup>-GAP50<sub>40-48</sub> tetramer staining of splenocytes isolated from infected C57Bl/6 mice at day 5 post-infection.

## METHODS

### Contact for Reagent and Resource Sharing

Further information and requests for resources and reagents should be directed to and will be fulfilled by the Lead Contact, John T. Harty ([john-harty@uiowa.edu](mailto:john-harty@uiowa.edu)).

### Experimental Model and Subject Details

C57Bl/6 (H-2<sup>b</sup>), BALB/c (H-2<sup>d</sup>) and CB6F1 (H-2<sup>bxd</sup>) mice were purchased from the National Cancer Institute (Frederick, MD). BALB.b (H-2<sup>b</sup>) and C57/L (H-2<sup>b</sup>) mice were purchased from the Jackson Laboratory (Bar Harbor, ME). All mice were housed with appropriate biosafety containment at the University of Iowa Animal Care Unit. The animals were treated and handled in accordance with guidelines established by the Institutional Animal Care and Use Committee. All experiments were performed using female mice, aged 6–8 weeks. *P. berghei* ANKA clone 234-parasitized *Anopheles stephensi* mosquitos were produced in house or obtained from New York University. For ECM infection, mice were injected intravenously (IV) with 10<sup>3</sup> viable sporozoites or intraperitoneally (IP) with 10<sup>6</sup> pRBCs. pRBCs were obtained from mice infected with a frozen stock 4–5 days previously. Numbers of transferred pRBCs were estimated by counting infected cells in Giemsa-stained blood smears. For virulent LM infection (*wt* or LM-GAP50<sub>40-48</sub>), BALB/c mice were infected IV with 5x10<sup>3</sup> CFU, and C57Bl/6 mice were infected IV with 10<sup>4</sup> CFU. Bacterial burden in the spleen was measured according to a previously published protocol (Badovinac and Harty, 2000).

### Method Details

#### *DC-LM immunizations*

For the purpose of TCR clonotyping, mice were immunized using a DC-LM prime-boost regimen (Badovinac et al., 2005). FMS-like tyrosine kinase-3 ligand (Flt-3L)-induced splenic DCs were LPS-matured, isolated after collagenase/DNAse digestion (Pham et al., 2009), and incubated with the following peptides for 2 h at a final concentration of 2 µM: TRAP<sub>130-138</sub> (SALLNUDNL), S20<sub>318-326</sub> (VNYSFLYLF) or GAP50<sub>40-48</sub> (SQLLNAKYL). CD11c<sup>+</sup> cells were then enriched using anti-CD11c MicroBeads (Miltenyi Biotec). A total

of  $5 \times 10^5$  purified DCs in saline were used to prime each mouse IV. After 7 days, mice were boosted IV with  $10^7$  CFU of recombinant attenuated LM-TRAP<sub>130-138</sub>, LM-S20<sub>318-326</sub> or LM-GAP50<sub>40-48</sub>. All recombinant attenuated LM strains were both *actA*- and *inlB*-deficient. The number of injected bacteria was verified by plating on tryptic soy agar supplemented with 50 µg/ml streptomycin.

#### *TCR clonotyping*

C57Bl/6 mice were immunized against GAP50<sub>40-48</sub> using the DC-LM prime-boost regimen. After 5 weeks, splenocytes were isolated and stained with LIVE/DEAD Fixable Aqua and anti-CD16/CD32 (FCR4G8; Thermo Fisher Scientific). Antigen-specific cells were labeled using a BV421-conjugated version of the GAP50<sub>40-48</sub> tetramer. Lineage markers were identified using anti-CD3-Cy5PE (17A2; BioLegend), anti-CD4-Alexa Fluor 700 (RM4-5; BD Biosciences) and anti-CD8-BV711 (53-6.7; BioLegend). Viable CD3<sup>+</sup> CD4<sup>-</sup> CD8<sup>+</sup> GAP50<sub>40-48</sub> tetramer<sup>+</sup> cells were then sorted at >98% purity using a custom-built 20-parameter FACS Aria II (BD Biosciences). TCR clonotyping was performed from 5,000 sorted cells per mouse using a template-switch anchored RT-PCR (Quigley et al., 2011). Amplicons were subcloned, sampled, sequenced and analyzed as described previously (Price et al., 2005). In all cases, TCR nomenclature was translated from the IMGT database via web-based alignment of molecular transcripts (<http://www.imgt.org>).

#### *Tetramer-based CD8<sup>+</sup> T cell enrichment*

The size of the naive antigen-specific CD8<sup>+</sup> T cell repertoire was quantified using a modified version of a previously published protocol (Moon et al., 2007). Spleen, popliteal, inguinal, brachial, axillary and cervical lymph nodes were isolated from naive mice and processed to a single cell suspension. Prepared cells were then labeled with an equimolar mixture of PE- and APC-conjugated tetramers representing each defined epitope. After incubation for 1 h at 4°C, cells were surface stained for CD8, CD90.2 and exclusion markers (B220, CD11b and CD11c). Labeled cells were subsequently captured and enumerated using anti-PE and anti-APC magnetic beads with an AutoMACS separator (Miltenyi Biotec).



### *Peptide mutants*

Mutant GAP50<sub>40-48</sub> peptides were generated by replacing individual amino acids with Ala or Ser (for P6-Ala), barring the anchor residues at P5 and P9 (BioSynthesis Inc.). Splenocytes were isolated from DC-LM-GAP50<sub>40-48</sub>-immunized mice during the memory phase (>40 days post-immunization) and restimulated for 5 h in the presence of brefeldin A with either *wt* or mutant peptides at a final concentration of 500 nM. All restimulations were performed in triplicate. IFN $\gamma$ -producing CD8<sup>+</sup> T cells were identified using a standard intracellular cytokine staining protocol (Doll et al., 2016). Data are expressed relative to the percentage of CD8<sup>+</sup> T cells producing IFN $\gamma$  in response to the *wt* peptide.

### *Generation of TCR $\beta$ retrogenic mice*

TCR $\beta$  retrogenic mice were generated on a C57Bl/6 background using retrovirus-mediated stem cell gene transfer (Bettini et al., 2013; Holst et al., 2006). The relevant antigen-specific TCR $\beta$  sequences were obtained from CD8<sup>+</sup> T cell clones derived from mice immunized with GAP50<sub>40-48</sub> (V $\beta$ 8.1<sup>+</sup>) or TRAP<sub>130-138</sub> (V $\beta$ 9<sup>+</sup>).

### *Isolation of mononuclear cells from the brains of *P. berghei* ANKA-infected mice*

Mononuclear cells were isolated from brain tissue using a previously published protocol with minor modifications (Zhao et al., 2009). Brains harvested after intravascular exclusion were processed and digested with collagenase D (1 mg/ml; Roche) and DNase (0.1 mg/ml; Sigma-Aldrich) for 30 min at 37°C. Dissociated brain tissue was then passed through a 70  $\mu$ m nylon mesh cell strainer, spun down, resuspended and centrifuged for 20 min over 37% Percoll. Mononuclear cells were collected from the pellet, and RBCs were lysed using 1X VitaLyse (CMDG).

### *Protein expression, purification and crystallization*

The  $\alpha$  and  $\beta$  chains of the TCR clones NB1, KL1 and KL4 were expressed separately as inclusion bodies and refolded with engineered disulfide linkages in the constant domains as described previously (Day et al., 2011). Ala substitutions in the H-2D<sup>b</sup> and

NB1 TCR sequences were introduced using site-directed mutagenesis. Soluble *wt* and mutant H-2D<sup>b</sup> heterodimers containing the GAP50<sub>40-48</sub> peptide were prepared as described previously (Day et al., 2011). Crystals of H-2D<sup>b</sup>-GAP50<sub>40-48</sub> (5 mg/ml) or the NB1 TCR in complex with H-2D<sup>b</sup>-GAP50<sub>40-48</sub> (6 mg/ml) in 10 mM Tris-HCl (pH 8) and 150 mM NaCl were grown by the hanging-drop, vapor-diffusion method at 20°C with a protein/reservoir drop ratio of 1:1. Crystals of free H-2D<sup>b</sup>-GAP50<sub>40-48</sub> were obtained in 0.1 M Tris-HCl (pH 8.5), 0.2 M lithium sulfate and 25–30% PEG8000. Crystals of the NB1 TCR in complex with H-2D<sup>b</sup>-GAP50<sub>40-48</sub> were obtained in 18% PEG3350, 2% ethylene glycol, 0.2 M CaCl<sub>2</sub> and 0.1 M HEPES (pH 7.2).

#### *Data collection and structure determination*

Crystals were soaked in a cryoprotectant solution containing mother liquor with the PEG8000 concentration increased to 30% (v/v) and then flash frozen in liquid nitrogen. Data were collected on the MX2 beamline at the Australian Synchrotron using the ADSC-Quantum 315r CCD detectors (at 100K). Data were processed with XDS software (Kabsch, 2010) and scaled using SCALA software (Evans, 2006) from the CCP4 suite (Collaborative Computational Project, 1994). The NB1 TCR structure was determined by molecular replacement using the Phaser program (Read, 2001) with the LC13 TCR as the search model (Protein Data Bank accession number, 1KGC) (Kjer-Nielsen et al., 2002), and the H-2D<sup>b</sup> structure was determined by molecular replacement using the Phaser program (Read, 2001) with H-2D<sup>b</sup> as the search model (Protein Data Bank accession number, 4L8D) (Valkenburg et al., 2013). Manual model building was conducted using Coot software (Emsley and Cowtan, 2004), followed by maximum-likelihood refinement with Buster. The NB1 TCR was numbered according to the IMGT unique numbering system (Lefranc, 2003). The final models were validated using the Protein Data Bank validation web site, and the final refinement statistics are summarized in Table S2. All molecular graphics representations were created using PyMol (DeLano, 2002).

#### *Surface plasmon resonance*

Surface plasmon resonance experiments were conducted at 25°C on a BIAcore 3000 instrument using 10 mM Tris-HCl (pH 8) and 150 mM NaCl supplemented with 1% BSA and 0.005% surfactant P20. The TCRs (*wt* or mutant) were immobilized on research-grade CM5 chips via standard amine coupling. All experiments were carried out at least twice in duplicate as described previously (Gras et al., 2009) across a H-2D<sup>b</sup>-GAP50<sub>40-48</sub> (*wt* or mutant) concentration range of 0.78–200 µM. Data were analyzed using BIAevaluation version 3.1 with the 1:1 Langmuir binding model.

### **Quantification and Statistical Analysis**

Statistical differences between two study groups were evaluated using an unpaired, two-tailed t test. Statistical differences between more than two study groups were evaluated using a one-way ANOVA with Tukey's multiple comparison post-hoc test. Bar graphs display mean ± SD for representative experiments and mean ± SEM for combined experiments. Statistical significance was assigned as \**p* < 0.05, \*\**p* < 0.01, \*\*\**p* < 0.001 and \*\*\*\**p* < 0.0001. Statistical analyses were performed using Prism 7 software (GraphPad).

### **Data and Software Availability**

Structural coordinates were submitted to the Protein Data Bank with accession codes 5WLI for H-2D<sup>b</sup>-GAP50<sub>40-48</sub> and 5WLG for the NB1 TCR in complex with H-2D<sup>b</sup>-GAP50<sub>40-48</sub>.

| REAGENT or RESOURCE  | SOURCE                      | IDENTIFIER      |
|--|-----------------------------|-----------------|
| <b>Antibodies</b>  |                             |                 |
| Anti-mouse CD8 $\alpha$<br>(clone 53-6.7)  | BioLegend                   | Cat# 100725     |
| Anti-mouse CD11a<br>(clone M17/4)  | BioLegend                   | Cat# 101107     |
| Anti-mouse CD90.2<br>(clone 30-H12)  | BioLegend                   | Cat# 105306     |
| Mouse V $\beta$<br>screening Panel<br>(V $\beta$ 2, 3, 4, 5.1, 5.2,<br>6, 7, 8.1/8.2, 8.3, 9,<br>10 <sup>b</sup> , 11, 12, 13, 14<br>and 17 <sup>a</sup> ) | BD Pharmingen               | Cat# 557004     |
| Anti-mouse IFN $\gamma$<br>(clone XMG1.2)  | BioLegend                   | Cat# 505809     |
| Anti-mouse CD5<br>(clone 53-7.3)   | BioLegend                   | Cat# 100629     |
| Anti-mouse CD44<br>(clone IM7)   | eBioscience                 | Cat# 11-0441-82 |
| Anti-mouse CD11b<br>(clone M1/70)  | eBioscience                 | Car# 45-0112-82 |
| Anti-mouse CD11c<br>(clone N418)   | eBioscience                 | Cat# 45-0114-82 |
| Anti-mouse B220<br>(clone RA3-6B2)   | eBioscience                 | Cat# 45-0452-82 |
| Anti-mouse CD3<br>(clone 17A2)   | BioLegend                   | Cat# 100309     |
| Anti-mouse CD4<br>(clone RM4-5)  | BD Bioscience               | Cat# 100536     |
| Anti-CD16/32<br>(clone FCR4G8)   | Thermo Fisher<br>Scientific | Cat# MFCR00     |
| <b>Tetramers</b>   |                             |                 |
| H-2D <sup>b</sup> -TRAP <sub>130-138</sub>   | <i>Prepared In house</i>    | NA              |
| H-2K <sup>b</sup> -S20 <sub>318-326</sub>  | <i>Prepared In house</i>    | NA              |
| H-2D <sup>b</sup> -GAP50 <sub>40-48</sub>  | <i>Prepared In house</i>    | NA              |
| H-2K <sup>b</sup> -OVA <sub>257-264</sub>  | <i>Prepared In house</i>    | NA              |
| H-2D <sup>b</sup> -GP <sub>33-41</sub>   | <i>Prepared In house</i>    | NA              |
| <b>Other reagents used for flow cytometry</b>  |                             |                 |
| LIVE/DEAD®<br>Fixable Aqua   | Thermo Fisher<br>Scientific | Cat# L34957     |
| Brilliant Violet<br>BV421™<br>Streptavidin   | BioLegend                   | Cat# 405225     |

| Chemical and Peptides                                 |                          |                 |
|---|--------------------------|-----------------|
| RNAlater® Stabilization Solution                      | Thermo Fisher Scientific | Cat# AM7020     |
| RNaseOUT™ Recombinant Ribonuclease Inhibitor          | Thermo Fisher Scientific | Cat# 10777019   |
| 10mM dNTP mix   | Thermo Fisher Scientific | Cat# 18427013   |
| SYBR® Gold Nucleic Acid Gel Stain                     | Thermo Fisher Scientific | Cat# S-11494    |
| S.O.C. medium   | Thermo Fisher Scientific | Cat# 15544034   |
| SYBR® Safe DNA Gel Stain                              | Thermo Fisher Scientific | Cat# S33102     |
| TrackIt™ Cyan/Orange Loading Buffer                   | Thermo Fisher Scientific | Cat# 10482-028  |
| GeneRuler 1kb DNA ladder, ready-to-use                | Thermo Fisher Scientific | Cat# SM0313     |
| LPS   | Sigma                    | Cat# L-8274     |
| Brefeldin A (1,000x)                                  | BioLegend                | Cat# 420601     |
| Collagenase Type II                                   | Gibco                    | Cat# 17101-015  |
| DNase   | Sigma-Aldrich            | Cat# D4513-1VL  |
| Percoll   | GE Healthcare            | Cat# 17-0891-01 |
| VitaLyse  | CMDG                     | Cat# WBL0100    |
| TRAP <sub>130-138</sub> peptide                       | BioSynthesis Inc         | Lot# T7825-2    |
| S20 <sub>318-326</sub> peptide                        | BioSynthesis Inc         | Lot# T7825-3    |
| GAP50 <sub>40-48</sub> peptide<br>SQLLNAKYL           | BioSynthesis Inc         | Lot# T7982      |
| GAP50 <sub>40-48</sub> peptide<br>mutant<br>AQLLNAKYL | BioSynthesis Inc         | Lot# P1168-1    |
| GAP50 <sub>40-48</sub> peptide<br>mutant<br>SALLNAKYL | BioSynthesis Inc         | Lot# P1168-2    |
| GAP50 <sub>40-48</sub> peptide<br>mutant<br>SQALNAKYL | BioSynthesis Inc         | Lot# P1168-3    |
| GAP50 <sub>40-48</sub> peptide<br>mutant<br>SQLANAKYL | BioSynthesis Inc         | Lot# P1168-4    |

|  |  |                            |
|--|--|----------------------------|
| GAP50 <sub>40-48</sub> peptide mutant<br>SQLLNAAAYL                                  | BioSynthesis Inc                               | Lot# P1168-5               |
| GAP50 <sub>40-48</sub> peptide mutant<br>SQLLNAKAL                                   | BioSynthesis Inc                               | Lot# P1168-6               |
| NB1, KL1 and KL4 TCR constructs  | DNA from Genscript                             | NA                         |
| H-2D <sup>b</sup> -GAP50 <sub>40-48</sub> , NB1, KL1 and KL4 TCR proteins            | In house                                       | Ref: (Day et al., 2011)    |
| <b>Commercial Assays</b>   |  |                            |
| anti-CD11c MicroBeads  | Miltenyi Biotec                                | Cat# 130-108-338           |
| Anti-PE MicroBeads   | Miltenyi Biotec                                | Cat# 130-048-801           |
| Anti-APC MicroBeads  | Miltenyi Biotec                                | Cat# 130-090-855           |
| μMACS mRNA isolation kit   | Milteniyi Biotec                               | Cat# 130-075-201           |
| SMARTer® RACE 5'/3' Kit  | Clontech                                       | Cat# 634859                |
| SuperScript® II Reverse Transcriptase  | Thermo Fisher Scientific                       | Cat# 18064014              |
| TOPO® TA Cloning® Kit for Sequencing with One Shot® MAX Efficiency® DH5α-T1R E. coli | Thermo Fisher Scientific                       | Cat# K459540               |
| <b>Deposited Data</b>  |  |                            |
| H-2D <sup>b</sup> -GAP50 <sub>40-48</sub> structure                                  | PDB web site                                   | <a href="#">PDB: 5WLI</a>  |
| NB1 TCR-H-2D <sup>b</sup> -GAP50 <sub>40-48</sub> structure                          | PDB web site                                   | <a href="#">PDB: 5WLG</a>  |
| <b>Experimental models: Cell lines</b>   |  |                            |
| Mouse: primary lymphocytes   | This manuscript                                | NA                         |
| Flt-3L tumor cell line   | Ref: (Mach et al., 2000)                       | B16-FLT3L (RRID:CVCL_IJ12) |
| <b>Experimental models: Organisms/Strains</b>  |  |                            |
| Mouse: C57BL/6J  | Harty Laboratory and National Cancer Institute | #556                       |

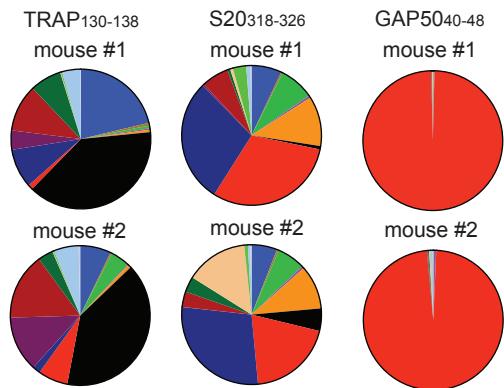
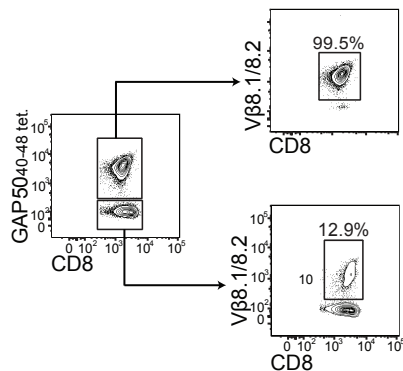
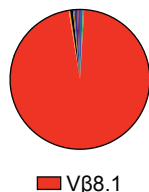
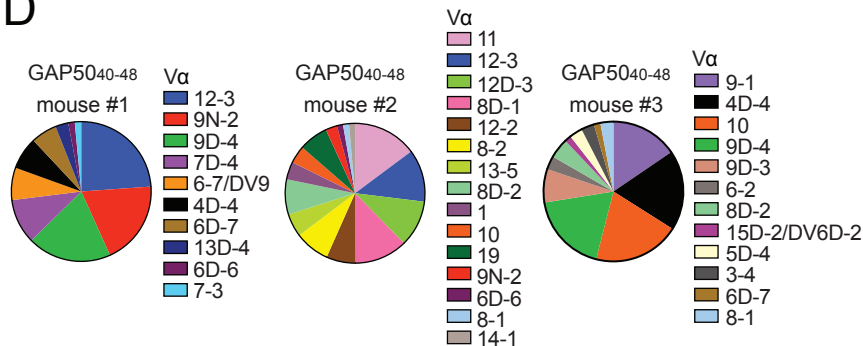
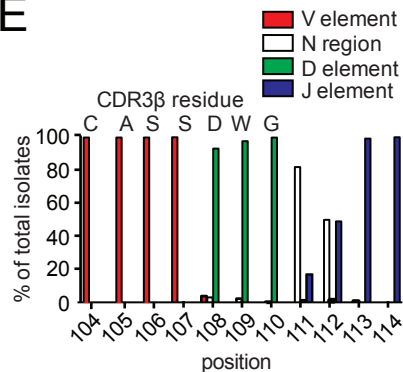
Deleted: PDB

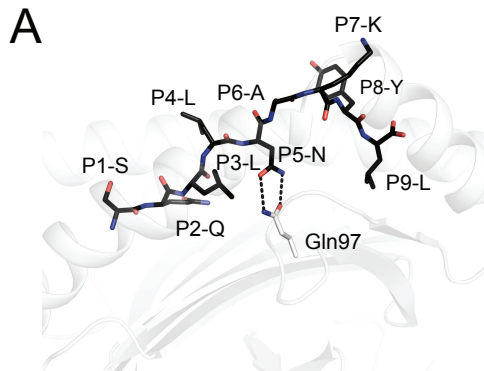
Deleted: PDB

|  |  |   |
|--|--|---|
| Mouse: CB6F1   | National Cancer Institute                            | #566  |
| Mouse: BALB/c  | Harty Laboratory and National Cancer Institute       | #555  |
| Mouse: BALB.b  | The Jackson Laboratory                               | 001952  |
| Mouse: (C57BL/6J x C57L) F1  | This manuscript                                      | NA  |
| Mouse: C57L  | The Jackson Laboratory                               | 000668  |
| Mouse: C57Bl/6 with GAP50 <sub>40-48</sub> -specific TCR $\beta$ chain retrogenic  | This manuscript                                      | NA  |
| Mouse: C57Bl/6 with TRAP <sub>130-138</sub> -specific TCR $\beta$ chain retrogenic | This manuscript                                      | NA  |
| <i>P. berghei</i> ANKA GFP-parasitized <i>Anopheles stephensi</i>                  | NYU Langone Health Insectary Core & Parasite Culture | NA  |
| Recombinant virulent <i>L. monocytogenes</i> -GAP50 <sub>40-48</sub>               | This manuscript                                      | NA  |
| Recombinant <i>actA-inlB- L. monocytogenes</i> -TRAP <sub>130-138</sub>            | Ref: (Doll et al., 2016)                             | NA  |
| Recombinant <i>actA-inlB- L. monocytogenes</i> -S20 <sub>318-326</sub>             | Ref: (Doll et al., 2016)                             | NA  |
| Recombinant <i>actA-inlB- L. monocytogenes</i> -GAP50 <sub>40-48</sub>             | Ref: (Doll et al., 2016)                             | NA  |
| <b>Software and Algorithms</b>   |  |   |
| Diva 8   | BD Biosciences                                       | <a href="http://www.bdbiosciences.com">http://www.bdbiosciences.com</a>               |
| Sequencher 5.2.3   | Gene Codes Corporation                               | <a href="http://www.genecodes.com/sequencher">http://www.genecodes.com/sequencher</a> |

|               |  |  |
|---------------|--|--|
| IMGT          | IMGT®, the international ImMunoGeneTics information system | <a href="http://www.imgt.org">http://www.imgt.org</a>  |
| XDS           | (Kabsch, 2010)   | Available online<br><a href="http://xds.mpimf-heidelberg.mpg.de/">http://xds.mpimf-heidelberg.mpg.de/</a>                            |
| Scala         | (Evans, 2006)  | Available online<br><a href="http://www.ccp4.ac.uk/html/scala.html">http://www.ccp4.ac.uk/html/scala.html</a>                        |
| CCP4          | (Collaborative Computational Project, 1994)                | Available online<br><a href="http://www.ccp4.ac.uk/">http://www.ccp4.ac.uk/</a>  |
| Phaser        | (Read, 2001)   | Available online<br><a href="http://www.ccp4.ac.uk/html/phaser.html">http://www.ccp4.ac.uk/html/phaser.html</a>                      |
| Coot          | (Emsley and Cowtan, 2004)                                  | Available online<br><a href="http://www2.mrc-lmb.cam.ac.uk/personal/pemsley/coot/">www2.mrc-lmb.cam.ac.uk/personal/pemsley/coot/</a> |
| Pymol         | (DeLano, W.L., 2002)                                       | Available online<br><a href="https://pymol.org/view">https://pymol.org/view</a>  |
| BIAevaluation | GE Healthcare  | Version 3.1<br><a href="https://www.biacore.com/lifesciences/">https://www.biacore.com/lifesciences/</a>                             |

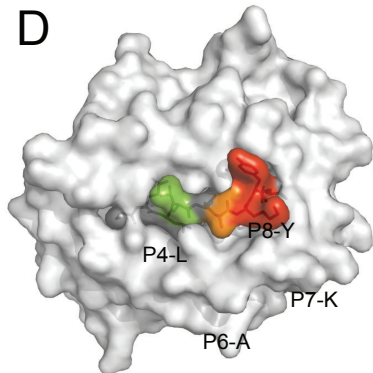
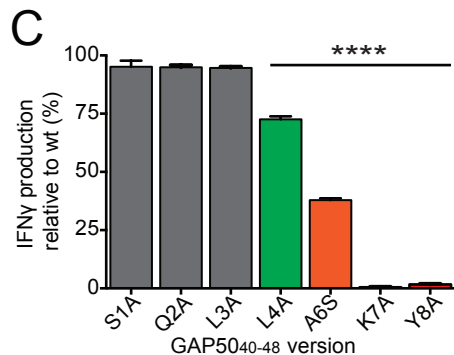


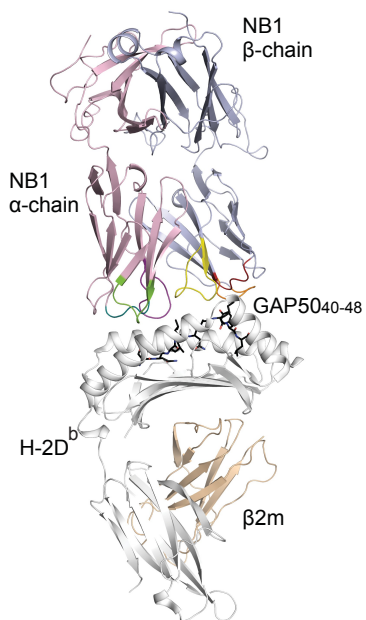
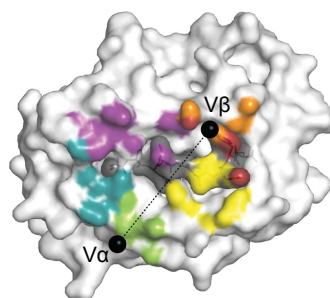
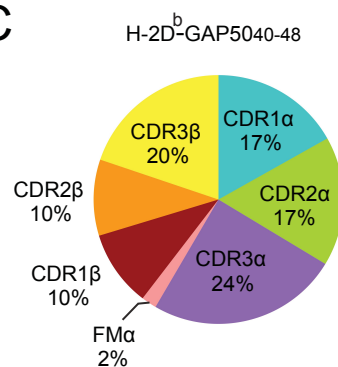
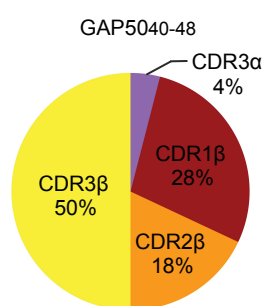
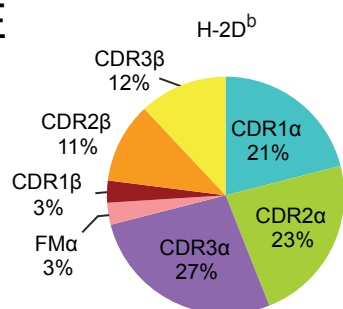
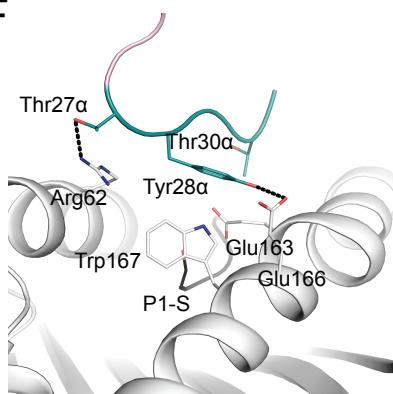
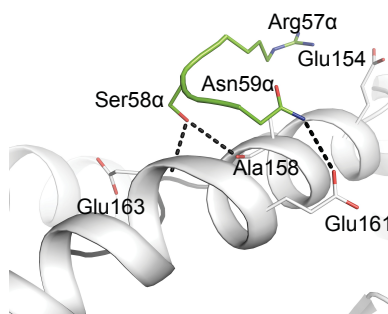
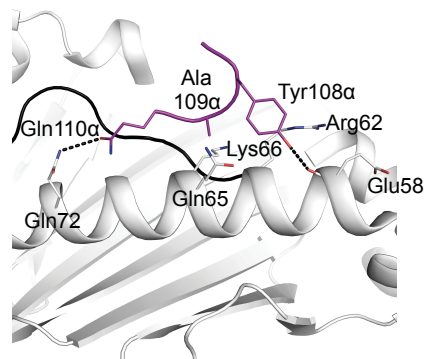
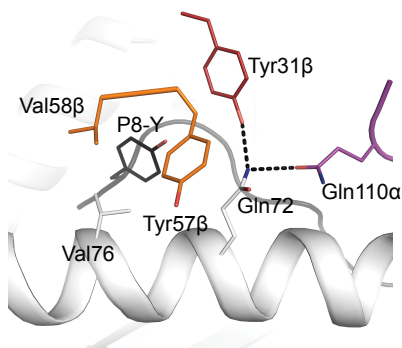
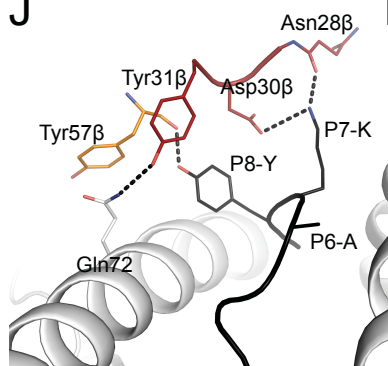
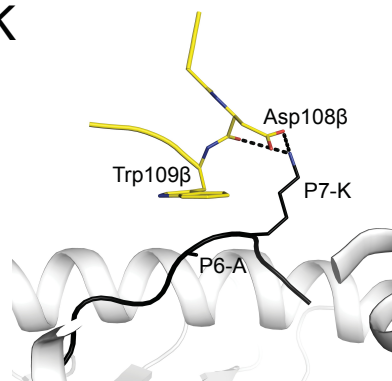
**A****B****C****D****E**



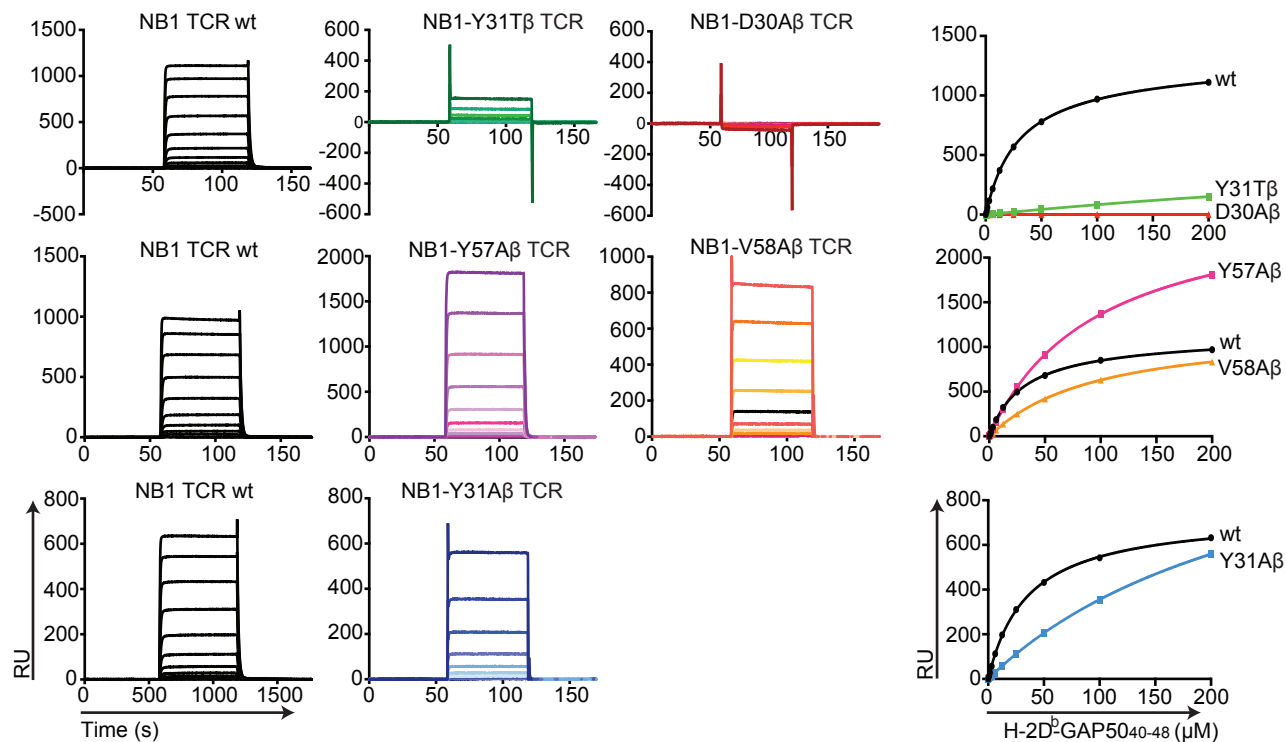
**B**

| GAP50 <sub>40-48</sub><br>version | amino acid<br>sequence                |
|-----------------------------------|---------------------------------------|
| wt                                | SQLLNAKYL                             |
| S1A                               | AQLLNAKYL                             |
| Q2A                               | SALLNAKYL                             |
| L3A                               | SQ <sup>A</sup> LLNAKYL               |
| L4A                               | SQ <sup>A</sup> LLN <sup>A</sup> AKYL |
| A6S                               | SQLLN <sup>S</sup> KYL                |
| K7A                               | SQLLN <sup>A</sup> AYL                |
| Y8A                               | SQLLN <sup>A</sup> K <sup>A</sup> L   |



**A****B****C****D****E****F****G****H****I****J****K**

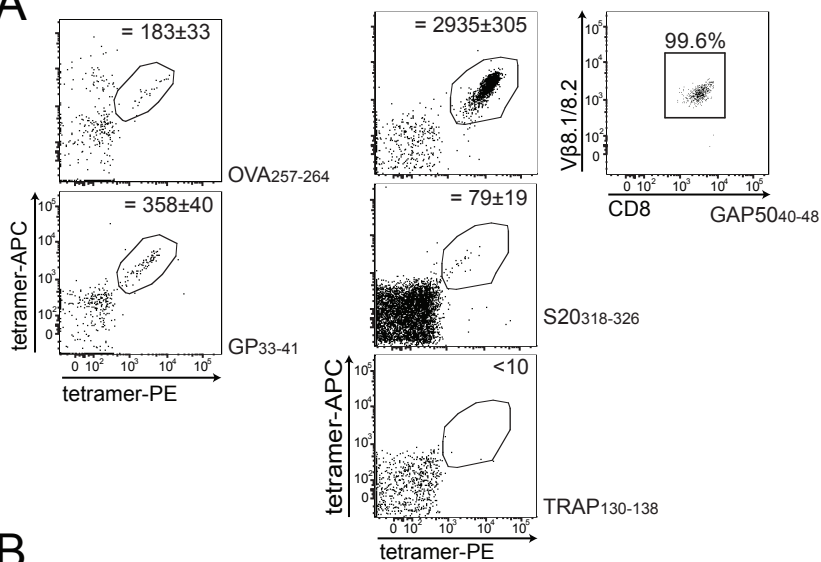
A



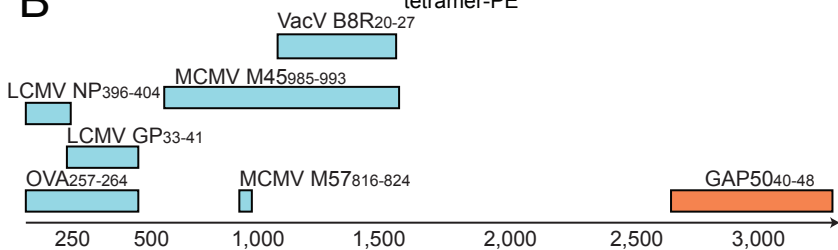
B

| NB1 TCR          | K <sub>deq</sub> ( $\mu$ M) |
|------------------|-----------------------------|
| wt               | 19.0 $\pm$ 0.3              |
| NB1 TCR mutants  | K <sub>deq</sub> ( $\mu$ M) |
| Tyr31Ala $\beta$ | > 200                       |
| Tyr31Thr $\beta$ | > 200                       |
| Asp30Ala $\beta$ | NB                          |
| Tyr57Ala $\beta$ | 59.0 $\pm$ 0.9              |
| Val58Ala $\beta$ | 59.7 $\pm$ 1.2              |

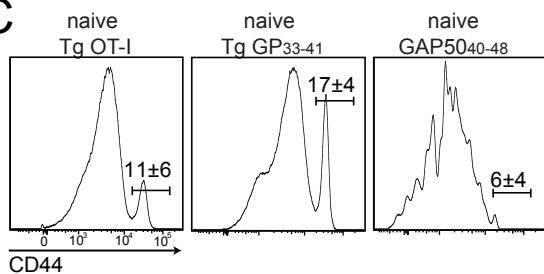
**A**



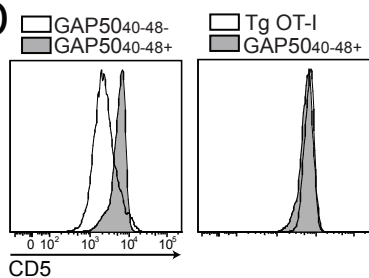
**B**

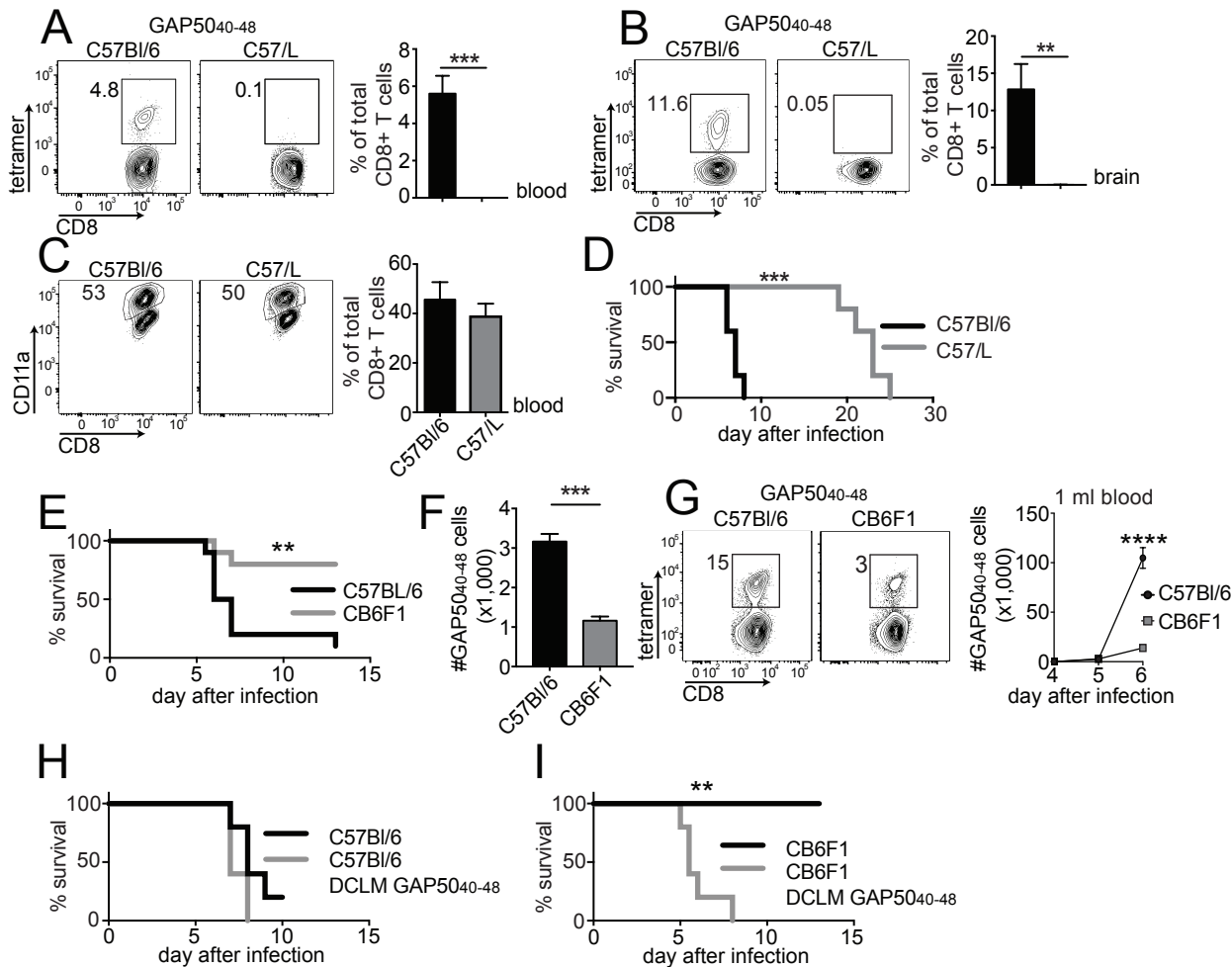


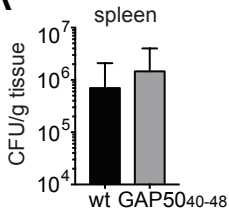
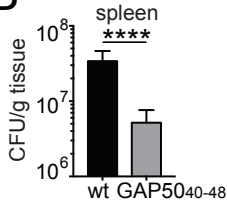
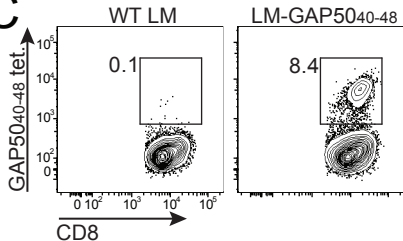
**C**



**D**





**A****B****C**

## SUPPLEMENTAL MATERIAL

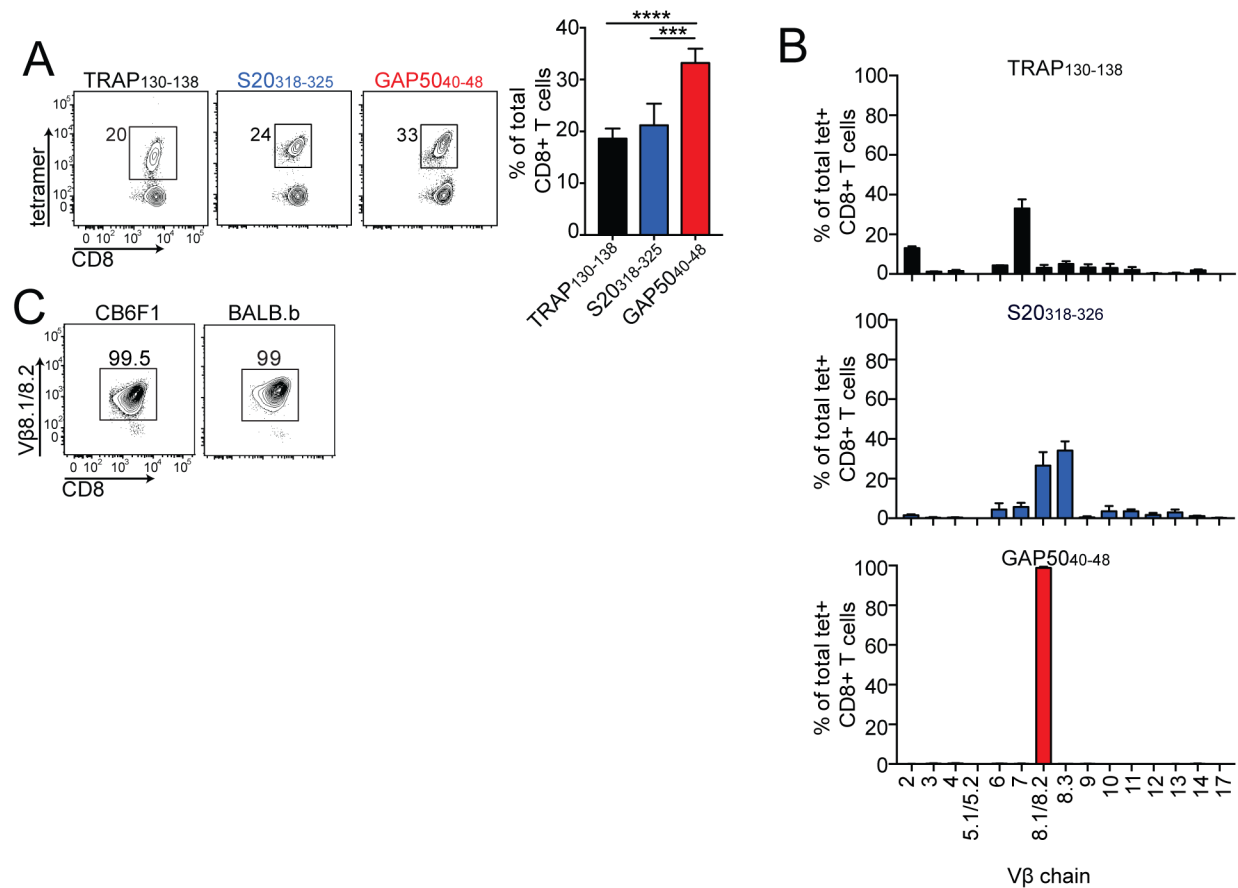


**Figure S1 related to Figure 1: TCR Vβ screening of CD8<sup>+</sup> T cell populations specific for TRAP<sub>130-138</sub>, S20<sub>318-326</sub> and GAP50<sub>40-48</sub>**

(A-B) Large CD8<sup>+</sup> T cell responses specific for TRAP<sub>130-138</sub>, S20<sub>318-326</sub> and GAP50<sub>40-48</sub> were generated in C57Bl/6 mice using a DC-LM prime-boost strategy. (A) The magnitude of each antigen-specific response was assessed at day 45 post-infection in the blood of immunized mice using the corresponding MHC I tetramer (representative flow cytometry plots – left; cumulative graphs – right). Data represent four independent experiments (n = 5 mice/group). Bar graphs depict mean ± SD. Significance was assessed using a one-way ANOVA with post-hoc Tukey's multiple comparison test (\*\*p<0.001, \*\*\*p<0.0001). (B) Distribution of various Vβ chains within different antigen-specific TCR repertoires, assessed in the blood of DC-LM-immunized mice and expressed as % of total tetramer<sup>+</sup> CD8<sup>+</sup> T cells. Data represent three independent experiments (n = 4–5 mice/group). Bars depict mean ± SD. (C) GAP50<sub>40-48</sub>-specific



CD8<sup>+</sup> T cell responses were generated in CB6F1 and BALB/b mice using a DC-LM prime-boost strategy. Representative flow cytometry plots show Vβ8.1/8.2 antibody staining of tetramer<sup>+</sup> cells in the blood of immunized mice. Data represent two independent experiments.

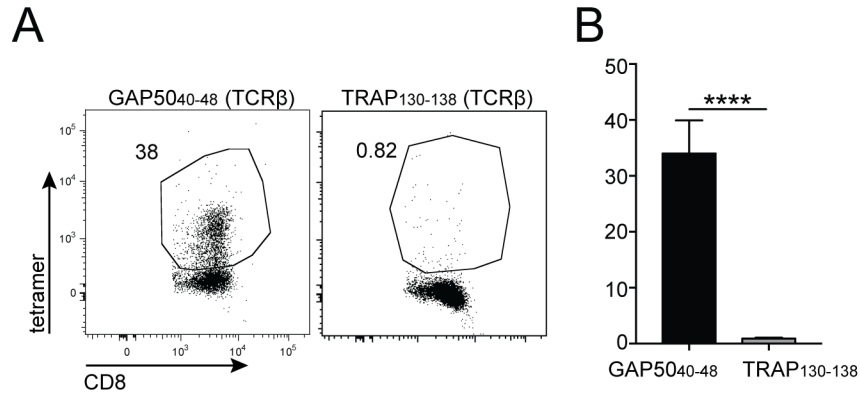


**Figure S2 related to Figure 1: Tetramer staining of retrogenic CD8<sup>+</sup> T cells**

(A, B) GAP50<sub>40-48</sub> and TRAP<sub>130-138</sub> TCRβ retrogenic mice were generated as described in the Methods. The success of TCR reconstitution was assessed in the blood of immunologically intact mice using specific MHC I tetramers (n = 5–6 mice/group). Representative flow cytometry plots (A) and cumulative graphs (B) showing tetramer staining of selected Vβ<sup>+</sup> CD8<sup>+</sup> T cells (Vβ8.1 for GAP50<sub>40-48</sub>, Vβ9 for TRAP<sub>130-138</sub>). Bars depict mean ± SD. Significance was assessed using a non-paired, two-tailed t test (\*\*\*\*p<0.0001).

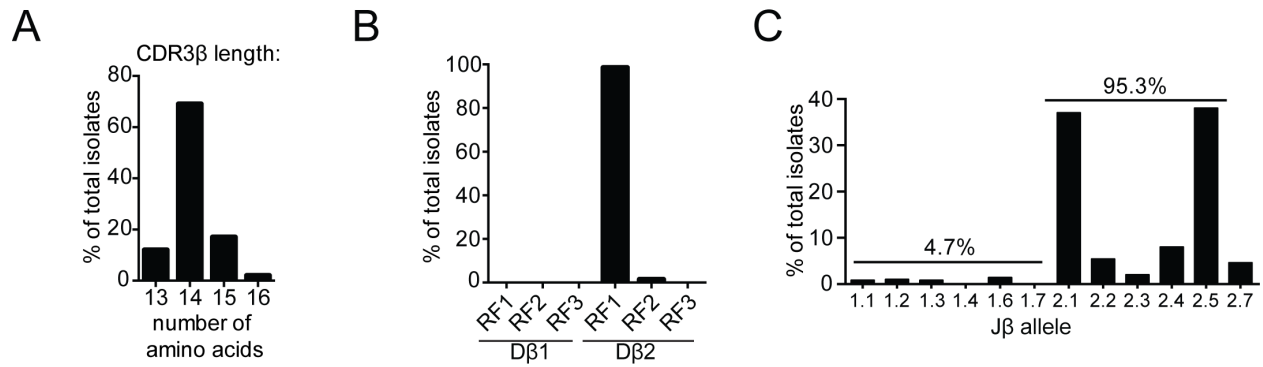


**Figure S3 related to Figure 1: Conserved features of the GAP50<sub>40-48</sub>-specific CDR3 β loop**

(A–D) Genetic material used for sequence analysis was derived from viable CD3<sup>+</sup> CD4<sup>−</sup> CD8<sup>+</sup> GAP50<sub>40-48</sub> tetramer<sup>+</sup> cells sorted from DC-LM-immunized mice. (A) Length distribution of CDR3β sequences expressed as % of total number of molecular Vβ8.1<sup>+</sup> clones (n = 5 mice). (B, C) Usage of Dβ and Jβ elements in CDR3β sequences expressed as % of total number of molecular Vβ8.1<sup>+</sup> clones (n = 5 mice).

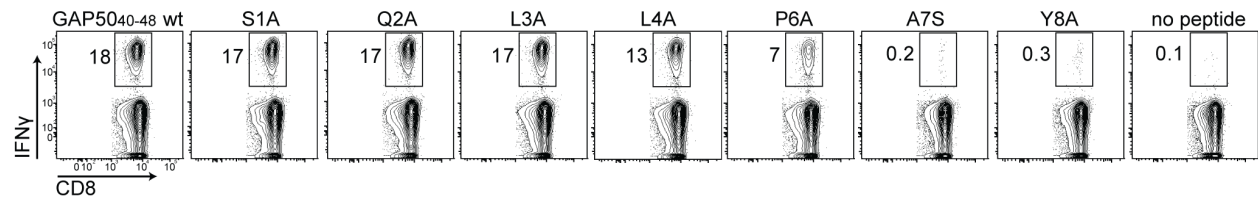


**Figure S4 related to Figure 2: Identification of GAP50<sub>40-48</sub> residues critical for TCR activation**

Representative flow cytometry plots showing IFN $\gamma$  staining of GAP50<sub>40-48</sub>-specific CD8<sup>+</sup> T cells isolated from DC-LM-immunized mice and subsequently restimulated *in vitro* with *wt* or mutant GAP50<sub>40-48</sub> peptides.

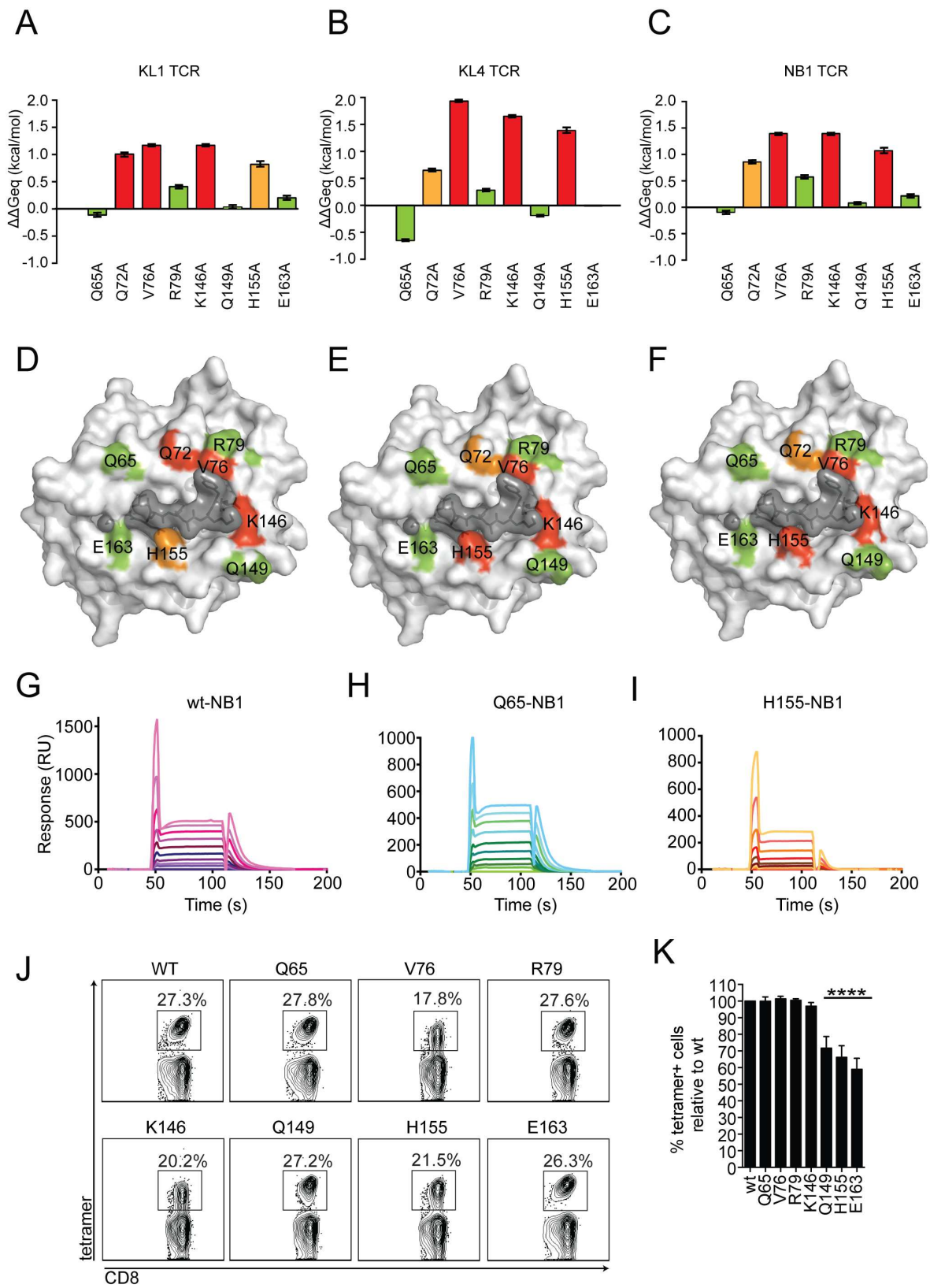


### Figure S5 related to Figure 3: Docking strategy of GAP50<sub>40-48</sub>-specific TCRs

(A–I) SPR analysis of GAP50<sub>40-48</sub>-specific TCRs isolated from the KL1, KL2 and NB1 CD8<sup>+</sup> T cell clones (Supplementary Table 5) to the indicated mutant H-2D<sup>b</sup> molecules presenting the GAP50<sub>40-48</sub> peptide. Ala mutations were introduced at selected sites based on the crystal structure of the NB1 TCR-H-2D<sup>b</sup>-GAP50<sub>40-48</sub> complex (Gln65, Val72, Gln72, Arg79, Lys146, His155 and Glu163). Ala mutation of Gln149 was used as a negative control. Ala substitutions were divided into 3 categories as follows: no impact (< 3-fold decrease in affinity) on TCR binding (green); moderate impact (3–5-fold decrease in affinity) on TCR binding (orange); and critical impact (> 5-fold decrease in affinity) on TCR binding (red). SPR results for H-2D<sup>b</sup> Ala mutants loaded with the *wt* GAP50<sub>40-48</sub> peptide are shown for the KL1 TCR (A), the KL4 TCR (B) and the NB1 TCR (C). Experiments were conducted in duplicate. Bars depict SD.  $\Delta\Delta G_{eq} = RT \cdot \ln(K_{deq}^{mut}/K_{deq}^{wt})$ , where *mut* designates mutant H-2D<sup>b</sup>. (D–F) The surface of H-2D<sup>b</sup> is shown in white, and the GAP50<sub>40-48</sub> peptide is shown in gray. (G–I) Representative SPR binding curves for the NB1 TCR with *wt* H-2D<sup>b</sup>-GAP50<sub>40-48</sub> (G), Q65A H-2D<sup>b</sup>-GAP50<sub>40-48</sub> (H) and H155A H-2D<sup>b</sup>-GAP50<sub>40-48</sub> (I). The H-2D<sup>b</sup>-GAP50<sub>40-48</sub> complexes were tested across a range of concentrations, indicated by the different colors, up to a maximum of 200  $\mu$ M). (J–K) Splenocytes isolated from GAP50<sub>40-48</sub>-immunized mice were stained with *wt* or mutant MHC I tetramers. Representative flow cytometry plots are shown in (J), and summary graphs are shown in (K). Data represent two independent experiments (n = 3 mice/group). Bars depict mean  $\pm$  SD. Significance was assessed using a one-way ANOVA (\*\*\*\*p<0.0001).

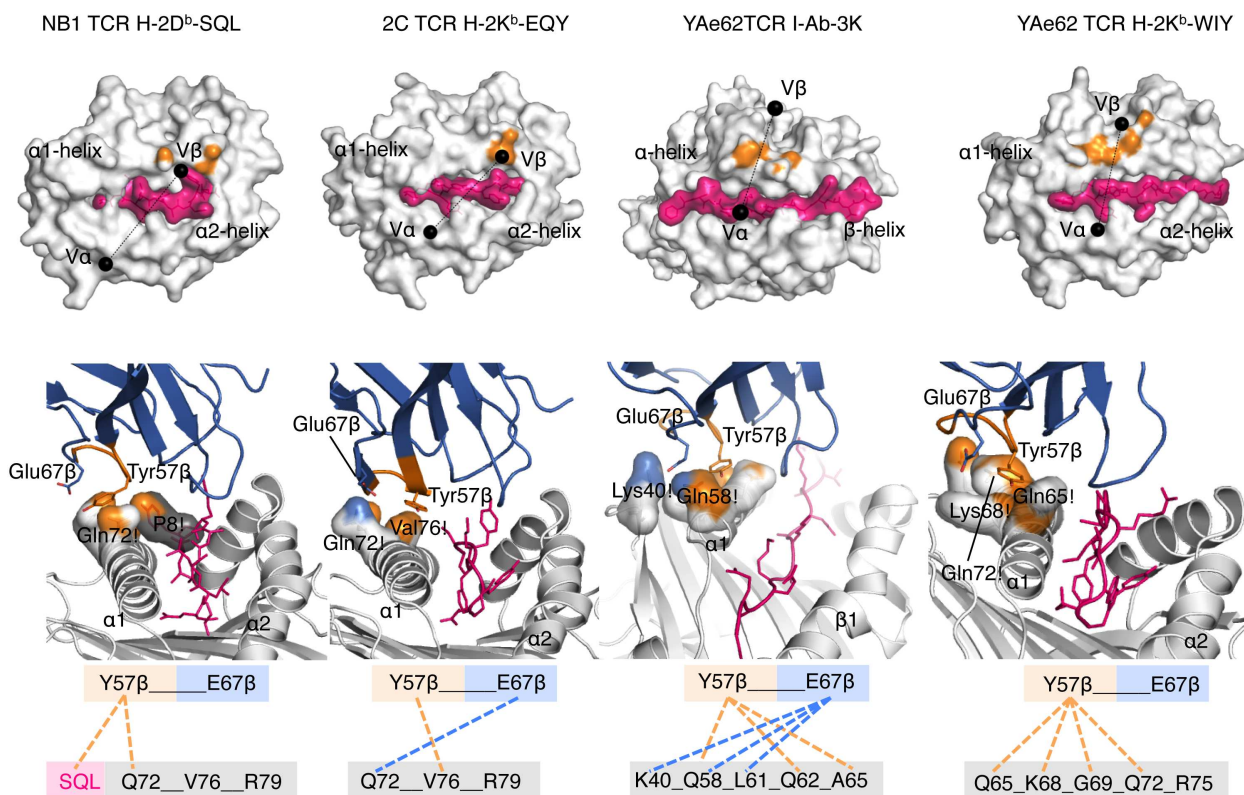


**Figure S6 related to Figure 3: Interaction of the conserved Y57 and E67 of the V $\beta$ 8 genes with MHC class I and II molecules**

From left to right: NB1 TCR-H-2D<sup>b</sup>-SQL, 2C TCR-H-2K<sup>b</sup>-EQY [PDB code: 2CKB, (Garcia et al., 1998)], YAe62 TCR-I-Ab-3K [PDB code: 3C60, (Dai et al., 2008)] and YAe62 TCR-H-2K<sup>b</sup>-WIY [PDB code: 3RGV, (Yin et al., 2011)] complexes. The Top panels represent the footprint of the CDR2 $\beta$  loop for each TCR (orange) on the surface of their respective peptide (pink) and MHC (white) surface.

The middle panels represent a close up view of the interactions between the CDR2 $\beta$  loop (orange) and FW $\beta$  (blue) with their peptide (pink stick) and MHC (white cartoon). The Tyr57 $\beta$  and the GLu67 $\beta$  are represented in stick, as well as the residues from the pMHC that are in contact with them.

The bottom panels show a representation of the interaction of the Tyr57 $\beta$  (orange dashes) and the Glu67 $\beta$  (blue dashes) with the residues from the peptide (pink box) and/or the MHC molecules (gray box).

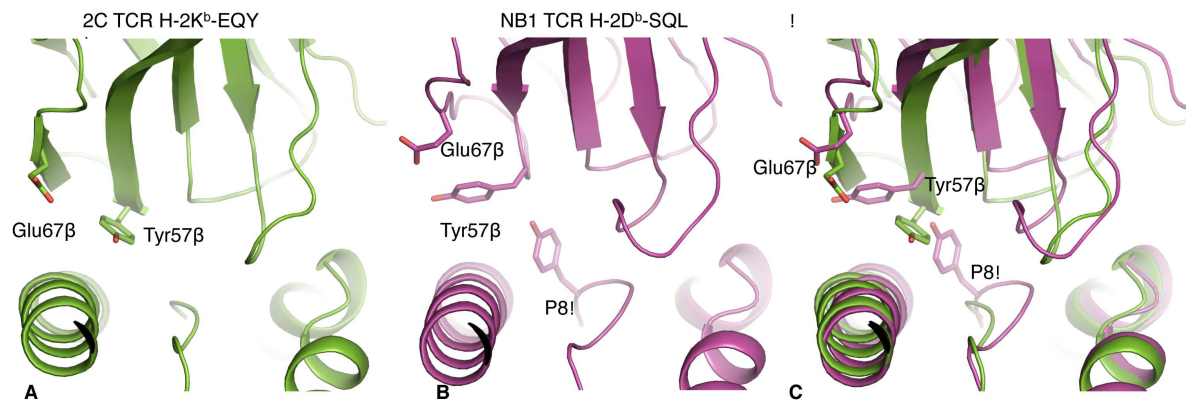


**Figure S7 related to Figure 3: Different location of the Tyr57 $\beta$  between V $\beta$ 8.2+ 2C TCR and the V $\beta$ 8.1+ NB1 TCR**

The panels show a close up view of the TCR Tyr57 $\beta$  and Glu67 $\beta$  interaction with the pMHC from the (A) 2C TCR-H-2K<sup>b</sup>-EQY [PDB code: 2CKB, (Garcia et al., 1998)] complex (green), (B) the NB1 TCR-H-2D<sup>b</sup>-SQL complex (purple), and (C) a superimposition of both of them. The C panel shows that the P8-Tyr of the SQL (purple stick) would clash with the location of the Tyr57 $\beta$  (green stick) of the 2C TCR.



**Table S1 related to Figure 1: CDR3 $\beta$  sequences of V $\beta$ 8.1<sup>+</sup> GAP50<sub>40-48</sub>-specific transcripts**

| CDR3 $\beta$ (amino acid) | CDR3 $\beta$ (nucleotide)                 | Counts |
|---------------------------|---|--------|
| CASSDWGTDAEQF             | tgtgccagcagtgattgggggacagatgctgagcagttc   | 93     |
| CASSDWGVQDTQY             | tgtgccagcagtgactgggggggtccaagacacccagttac | 21     |
| CASSDWGVQDTQY             | tgtgccagcagtgattgggggggtccaagacacccagttac | 20     |
| CASSDWGNQDTQY             | tgtgccagcagtgattgggggaaccaagacacccagttac  | 16     |
| CASSDWGVQDTQY             | tgtgccagcagtgactgggggggtccaagacacccagttac | 14     |
| CASSDWGNIAEQF             | tgtgccagcagtgactgggggaactatgctgagcagttc   | 11     |
| CASSDWGVQDTQY             | tgtgccagcagtgactgggggggtccaagacacccagttac | 11     |
| CASSDWGNQDTQY             | tgtgccagcagtgactgggggaaccaagacacccagttac  | 8      |
| CASSDWGGQNTLY             | tgtgccagcagtgactgggggggaggtcaaaacaccttg   | 8      |
| CASSDWGNQDTQY             | tgtgccagcagtgattggggtaaccaagacacccagttac  | 6      |
| CASSDWGRDAEQF             | tgtgccagcagtgactggggggcgagatgctgagcagttc  | 5      |
| CASSHWGGDTQYF             | tgtgccagcagccactgggggtggggacacccagttacttt | 5      |
| CASSDWGNTGQLY             | tgtgccagcagtgactgggggaacacccgggcagctctac  | 4      |
| CASSDWGVEQY               | tgtgccagcagtgactggggggggcgtgaacagttacagt  | 4      |
| CASSDWGASSYEQY            | tgtgccagcagtgattggggggcgagctcctatgaacag   | 3      |
| CASSDWGVDAEQF             | tgtgccagcagtgactgggggggtagatgctgagcagttc  | 3      |
| CASSDWGNIAEQF             | tgtgccagcagtgattggggaaactatgctgagcagttc   | 3      |
| CASSDWGGQNTLY             | tgtgccagcagtgattggggggggcgtcaaaacaccttg   | 3      |
| CASSDFGTADTEVF            | tgtgccagcagtgattcgggacagcggacacagaagtc    | 2      |
| CASSDWGAQDTQY             | tgtgccagcagtgactggggagcccaagacacccagttac  | 2      |
| CASSDWGGAYEQY             | tgtgccagcagtgactggggggggcgctatgaacagttac  | 2      |
| CASSDWGSGNTLY             | tgtgccagcagtgattgggggctggaaatacgtctat     | 2      |
| CASSDWGGQDTQYF            | tgtgccagcagtgactggggggggacaagacacccagttac | 2      |
| CASSDWGGQNTLY             | tgtgccagcagtgactgggggggggtcaaaacaccttgtag | 2      |
| CASSDWGGYAEQFF            | tgtgccagcagtgactggggggggctatgctgagcagttc  | 2      |
| CASSDWGQDTQY              | tgtgccagcagtgactgggggcaagacacccagttacttt  | 2      |
| CASSDWGTSPLY              | tgtgccagcagtgactgggggacctctccttgtagcttt   | 2      |
| CASSDWGNIAEQF             | tgtgccagcagtgactgggggaactatgctgagcagttc   | 2      |
| CASSDWGGSQNTLY            | tgtgccagcagtgattggggggggaggtcaaaacaccttg  | 2      |
| CASSDWGAAGNTLY            | tgtgccagcagtgattggggggcggtggaaatacgtctc   | 1      |
| CASSDWGIYAEQFF            | tgtgccagcagtgattgggggatctatgctgagcagttc   | 1      |
| CASSDWGGQSDYT             | tgtgccagcagtgattggggacagggctccgactacacc   | 1      |
| CASSDFQQDTQYF             | tgtgccagcagtgattccagcaagacacccagttacttt   | 1      |
| CASSDWGGAETLY             | tgtgccagcagtgactggggggggcgagaaacgctgtat   | 1      |
| CASSDWGDTGQLY             | tgtgccagcagtgactgggggggacacccgggcagctctac | 1      |
| CASSDWGGVEQY              | tgtgccagcagtgactggggggggcgtgaacagttacagt  | 1      |
| CASSDWGGQNTLY             | tgtgccagcagtgactggggggggacaaaacaccttgtag  | 1      |
| CASSDWGNIAEQF             | tgtgccagcagtgactgggggaactatgctgagcagttc   | 1      |
| CASSDWGSAETLY             | tgtgccagcagtgattgggggagtcagaaacgctgtat    | 1      |
| CASSDWGSGQNTLY            | tgtgccagcagtgattggggtagtcaaaacaccttgtag   | 1      |
| CASSDWGVYAEQF             | tgtgccagcagtgactgggggggtctatgctgagcagttc  | 1      |

Blue: *V* gene; red: *D* gene; black: N insertion; purple, green, gray, orange, pale blue and pink: *J* genes.

**Table S2 related to Figures 2 and 3: Data collection and refinement statistics**

| <b>Data collection</b>                      | <b>H-2D<sup>b</sup>-GAP50<sub>40-48</sub></b> | <b>NB1 TCR-H-2D<sup>b</sup>-GAP50<sub>40-48</sub></b> |
|---|---|---|
| Temperature (K)                             | 100   | 100   |
| Resolution range (Å)                        | 48.56 - 2.20<br>(2.27 - 2.20)                 | 38.82 - 2.1<br>(2.175 - 2.1)                          |
| Space group                                 | <i>P2<sub>1</sub></i>                         | <i>P2<sub>1</sub></i>                                 |
| Unit cell (Å)<br>(°)                        | 53.27, 159.92, 108.46<br>β= 92.33             | 115.74, 70.21, 116.49<br>β= 108.28                    |
| Total reflections                           | 181134 (17680)                                | 206330 (20547)  |
| Unique reflections                          | 91389 (9050)                                  | 103825 (10315)  |
| Multiplicity                                | 2.0 (2.0)                                     | 2.0 (2.0)   |
| Data Completeness (%)                       | 99.61 (97.23)                                 | 100 (100)   |
| <i>I</i> /σ( <i>I</i> )                     | 16.10 (4.31)                                  | 15.61 (2.42)  |
| <i>R</i> <sub>pim</sub> <sup>a</sup> (%)    | 3.9 (24.0)                                    | 3.4 (34.6)  |
| <b>Refinement statistics</b>                |   |   |
| <i>R</i> <sub>factor</sub> <sup>b</sup> (%) | 19.4  | 19.3  |
| <i>R</i> <sub>free</sub> <sup>b</sup> (%)   | 24.1  | 23.5  |
| <i>Non-hydrogen atoms</i>                   |   |   |
| Protein                                     | 12641   | 12906   |
| Water                                       | 1262  | 890   |
| <i>Rms deviation from ideality</i>          |   |   |
| Bonds lengths (Å)                           | 0.01  | 0.01  |
| Bonds angles (°)                            | 1.13  | 1.14  |
| <i>Ramachandran plot (%)</i>                |   |   |
| Favored                                     | 99.3  | 95.0  |
| Outliers                                    | 0   | 0.8   |

$$^a R_{pim} = \sum_{hkl} [1 / (N-1)]^{1/2} \sum_i |I_{hkl,i} - \langle I_{hkl} \rangle| / \sum_i \langle I_{hkl} \rangle$$

<sup>b</sup>  $R_{factor} = \sum_{hkl} ||F_o| - |F_c|| / \sum_{hkl} |F_o|$  for all data except 5% which were used for *R*<sub>free</sub> calculation. Values in parentheses represent the highest resolution-shell.

**Table S3 related to Figure 3 and S5: CDR3 sequences of GAP50<sub>40-48</sub> specific TCR clones**

| TCR | V $\alpha$ | CDR3 $\alpha$   | V $\beta$ | CDR3 $\beta$             |
|-----|------------|-----------------|-----------|--------------------------|
| NB1 | 18         | CATVYAQGLTF     | 8.1       | CASS <b>DW</b> GD TGQLYF |
| KL1 | 17.1       | CAMSPQGGS AKLIF | 8.1       | CASS <b>DW</b> GNQDTQYF  |
| KL4 | 18         | CATEGNNAGAKLTF  | 8.1       | CASS <b>DW</b> GNQDTQYF  |

In IMGT nomenclature, V $\alpha$ 17.1 corresponds to TRAV16D/DV11, V $\alpha$ 18 corresponds to TRAV8-2, and V $\beta$ 8.1 corresponds to TRBV13-3.

**Table S4 related to Figure 3: Contacts between the NB1 TCR and the H-2D<sup>b</sup>-GAP50<sub>40-48</sub> complex**

| TCR region       | TCR residues          | H-2D <sup>b</sup> residues              | Bond type |
|------------------|-----------------------|---|-----------|
| CDR1 $\alpha$    | Thr27-O $\gamma$ 1    | Arg62-NH2                               | VDW, HB   |
| CDR1 $\alpha$    | Tyr28-OH              | Glu163, Glu166-O $\epsilon$ 2, Trp167   | VDW, HB   |
| CDR1 $\alpha$    | Thr30                 | Glu163                                  | VDW       |
| CDR2 $\alpha$    | Arg57                 | Ala158                                  | VDW       |
| CDR2 $\alpha$    | Ser58-O $\gamma$      | Ala158-O, Gly162, Glu163-N              | VDW, HB   |
| CDR2 $\alpha$    | Asn59-N $\delta$ 2    | Ala158, Glu161-O $\epsilon$ 1, Gly162   | VDW, HB   |
| CDR3 $\alpha$ -J | Tyr108-OH             | Glu58-O, Arg62, Gln65                   | VDW, HB   |
| CDR3 $\alpha$ -J | Ala109                | Arg62, Lys66                            | VDW       |
| CDR3 $\alpha$ -J | Gln110-O $\epsilon$ 1 | Gly69, Gln72-N $\epsilon$ 2             | VDW, HB   |
| CDR1 $\beta$     | Tyr31-OH              | Gln72-N $\epsilon$ 2                    | VDW, HB   |
| CDR2 $\beta$     | Tyr57                 | Gln72, Val76                            | VDW       |
| CDR2 $\beta$     | Val58                 | Val76, Arg79                            | VDW       |
| CDR3 $\beta$ -D  | Asp108-O $\delta$ 2   | Ser150-O                                | VDW, HB   |
| CDR3 $\beta$ -D  | Trp109                | Ser150, Gly151, His155                  | VDW       |
| CDR3 $\beta$ -J  | Thr112-O $\gamma$ 1   | His155-N $\epsilon$ 2                   | VDW, HB   |
| TCR region       | TCR residues          | GAP50 <sub>40-48</sub> peptide residues | Bond type |
| CDR3 $\alpha$ -J | Ala109                | Leu4                                    | VDW       |
| CDR3 $\alpha$ -J | Gln110                | Leu4                                    | VDW       |
| CDR1 $\beta$     | Asn28-O               | Lys7-NZ                                 | VDW, HB   |
| CDR1 $\beta$     | Asp30-O $\delta$ 2    | Lys7-NZ, Tyr8                           | VDW, SB   |
| CDR1 $\beta$     | Tyr31                 | Tyr8                                    | VDW       |
| CDR2 $\beta$     | Tyr57-O               | Tyr8-OH                                 | VDW, HB   |
| CDR3 $\beta$ -D  | Asp108-O $\delta$ 1-O | Lys7-NZ                                 | VDW, SB   |
| CDR3 $\beta$ -D  | Trp109                | Ala6                                    | VDW       |

CDR: complementary-determining regions; HB: hydrogen bonds (cut-off = 3.5 Å),  
VDW: van der Waals (cut-off = 4 Å), SB: salt bridge (cut-off = 5Å).

**Table S5 related to Figures 3 and S5: Equilibrium binding affinities of different GAP50<sub>40-48</sub>-specific TCRs and selected H-2D<sup>b</sup> Ala mutants loaded with *wf* peptide**

| MHCp complex                                    | KL1 TCR<br>(K <sub>deg</sub> $\mu$ M) | KL4 TCR<br>(K <sub>deg</sub> $\mu$ M) | NB1 TCR<br>(K <sub>deg</sub> $\mu$ M) |
|---|---------------------------------------|---------------------------------------|---------------------------------------|
| H-2D <sup>b</sup> -GAP50 <sub>40-48</sub>       | 27.8 $\pm$ 0.3                        | 7.5 $\pm$ 0.2                         | 19.0 $\pm$ 0.3                        |
| H-2D <sup>b</sup> -Q65A-GAP50 <sub>40-48</sub>  | 23.1 $\pm$ 1.0                        | 2.5 $\pm$ 0.1                         | 16.3 $\pm$ 0.3                        |
| H-2D <sup>b</sup> -Q72A-GAP50 <sub>40-48</sub>  | 152.0 $\pm$ 4.0                       | 22.4 $\pm$ 0.2                        | 80.5 $\pm$ 1.3                        |
| H-2D <sup>b</sup> -V76A-GAP50 <sub>40-48</sub>  | > 200                                 | 196.0 $\pm$ 2.0                       | > 200                                 |
| H-2D <sup>b</sup> -R79A-GAP50 <sub>40-48</sub>  | 55.6 $\pm$ 1.0                        | 12.0 $\pm$ 0.2                        | 50.0 $\pm$ 1.4                        |
| H-2D <sup>b</sup> -K146A-GAP50 <sub>40-48</sub> | > 200                                 | 121.5 $\pm$ 3.5                       | > 200                                 |
| H-2D <sup>b</sup> -Q149A-GAP50 <sub>40-48</sub> | 29.3 $\pm$ 0.7                        | 5.5 $\pm$ 0.1                         | 21.8 $\pm$ 0.2                        |
| H-2D <sup>b</sup> -H155A-GAP50 <sub>40-48</sub> | 111.0 $\pm$ 11.0                      | 77.7 $\pm$ 3.6                        | 115.5 $\pm$ 11.5                      |
| H-2D <sup>b</sup> -E163A-GAP50 <sub>40-48</sub> | 39.2 $\pm$ 2.1                        | 7.4 $\pm$ 0.1                         | 27.4 $\pm$ 1.0                        |

Data represent at least two independent experiments performed in duplicate using surface plasmon resonance (mean  $\pm$  SEM).

**Table S6A related to Figure 4: Mouse CDR1 $\beta$  sequence alignment**

| Mouse V $\beta$ | CDR1 $\beta$  |
|-----------------|---------------|
| 8.1             | NNH <b>DY</b> |
| 10.1            | LGH <b>DT</b> |
| 28.1            | MKH <b>DS</b> |
| 13.1            | SGH <b>DT</b> |
| 9.1             | MNH <b>DT</b> |
| 6.1             | FNH <b>DT</b> |

CDR1  $\beta$  residues of the V $\beta$ 8.1<sup>+</sup> NB1 TCR critical for H-2D<sup>b</sup>-GAP50<sub>40-48</sub> recognition are depicted in red (Asp30 $\beta$  and Tyr31 $\beta$ ). Listed are mouse V $\beta$  gene segments with a common Asp30 $\beta$  residue (in bold). Tyr31 $\beta$  is unique to the V $\beta$  8.1 gene.

**Table S6B related to Figure 4: Mouse CDR2 $\beta$  sequence alignment**

| Mouse V $\beta$ | CDR2 $\beta$    |
|-----------------|-----------------|
| 8.1             | S <b>YV</b> ADS |
| 15.1            | STVNSAI         |
| 1.1             | YSV <b>K</b> QL |

CDR2 $\beta$  residues of the V $\beta$ 8.1<sup>+</sup> NB1 TCR moderately important for H-2D<sup>b</sup>-GAP50<sub>40-48</sub> recognition are depicted in blue (Tyr57 $\beta$  and Val58 $\beta$ ). Listed are mouse V $\beta$  gene segments with a common Val58 $\beta$  residues (in bold).